AD-A090 050 PURDUE UNIV LAFAYETTE IND SCHOOL OF AERONAUTICS AND --ETC F/G 5/8
MULTIVARIABLE CLOSED-LOOP ANALYSIS AND FLIGHT CONTROL SYNTHESIS--ETC(U)
JUN 80 D K SCHMIDT AFOSR-79-0042

UNCLASSIFIED AFOSR-TR-80-0961 NL

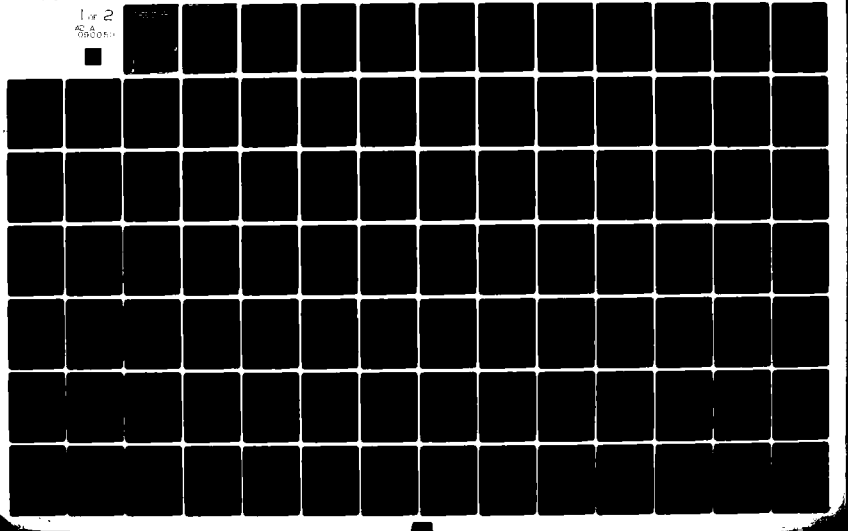

AFOSR-TR-80-0981

LEVEL II

MULTIVARIABLE CLOSED-LOOP ANALYSIS AND FLIGHT CONTROL SYNTHESIS FOR AIR-TO-AIR TRACKING

by

David K. Schmidt
School of Aeronautics and Astronautics
Purdue University
West Lafayette, IN 47907

Final Report

Prepared for the
Air Force Office of Scientific Research
Air Force Systems Command
Boiling AFB, DC 20332

June 18, 1980

AIR FORCE OFFICE OF SCIENTIFIC RESEARCH (AFSC)
NOTICE OF TRANSMITTAL TO DDC
This technical report has been reviewed and is approved for public release IAW AFR 190-12 (7b).
Distribution is unlimited.
A. D. BLOSE
Technical Information Officer

Unclassified

SECURITY CLASSIFICATION OF THIS PAGE (When Data Entered)

REPORT DOCUMENTATION PAGE	READ INSTRUCTIONS BEFORE COMPLETING FORM
1. REPORT NUMBER: AFOSR-TR-80-0961	2. GOVT ACCESSION NO.: A090 050 / 3. RECIPIENT'S CATALOG NUMBER
4. TITLE (and Subtitle): MULTIVARIABLE CLOSED-LOOP ANALYSIS AND FLIGHT CONTROL SYNTHESIS FOR AIR-TO-AIR TRACKING	5. TYPE OF REPORT & PERIOD COVERED: Final Report, 1 Jan 79 — 31 Dec 79 / 6. PERFORMING ORG. REPORT NUMBER
7. AUTHOR(s): David K. Schmidt	8. CONTRACT OR GRANT NUMBER(s): AFOSR-79-0042
9. PERFORMING ORGANIZATION NAME AND ADDRESS: School of Aeronautics and Astronautics, Purdue University, West Lafayette, IN 47907	10. PROGRAM ELEMENT, PROJECT, TASK AREA & WORK UNIT NUMBERS: 61102F 2313/D9
11. CONTROLLING OFFICE NAME AND ADDRESS: AFOSR, Bolling AFB, DC 20332 (NL)	12. REPORT DATE: 18 June 1980 / 13. NUMBER OF PAGES: 102
14. MONITORING AGENCY NAME & ADDRESS (if different from Controlling Office)	15. SECURITY CLASS. (of this report): Unclassified / 15a. DECLASSIFICATION/DOWNGRADING SCHEDULE

16. DISTRIBUTION STATEMENT (of this Report)

Approved for public release; distribution unlimited

17. DISTRIBUTION STATEMENT (of the abstract entered in Block 20, if different from Report)

18. SUPPLEMENTARY NOTES

19. KEY WORDS (Continue on reverse side if necessary and identify by block number)

Man-Machine Dynamics
Pilot Modeling
Flight Control Synthesis
Handling Qualities
Multivariable Control Theory

20. ABSTRACT (Continue on reverse side if necessary and identify by block number)

A synthesis method based on optimal control techniques, closed-loop task-oriented design objectives, and an optimal control model of the human pilot was applied to augment the system dynamics in the air-to-air tracking task. Single and multi-axis analyses were performed. Single axis results, obtained for longitudinal pitch tracking with different sets of active sight display dynamics, indicate the optimum system dynamics were affected by numerator (or display) dynamics. Improved tracking performance was predicted, and the

DD FORM 1 JAN 73 1473

Unclassified

SECURITY CLASSIFICATION OF THIS PAGE (When Data Entered)

20 continued

trends in augmented system dynamics (eigenvalues) were shown to agree with previous results. Moving-base simulation results obtained for a highly-banked flight condition were used to also establish a new multi-axis pilot model. This model is considered suitable for simultaneous control of the dynamically interacting longitudinal and lateral-directional axes of the vehicle/display system. The system augmentation, based on this model, again was predicted to significantly improve performance. The trends in system eigenvalues for various augmentation levels showed good agreement with the above longitudinal results. However, the lateral-directional axis was found to be much more important, and significant modification of the dynamics were predicted to lead to system improvements.

FORWARD

This research was performed for the Air Force Office of Scientific Research under Grant No. AFOSR-79-0042. Dr. Al Fregly (AFOSR/NL) was the technical program manager. The work was initiated while the author was a participant in the AFOSR-ASEE Summer Faculty Program at the Air Force Flight Dynamics Laboratory. Mr. Frank George of the Flight Dynamics Laboratory (now AFWAL/FIGC)was the Laboratory technical monitor for the entire project. The author is indebted to Dr. Fregly, Mr. George and to Mr. Ron Anderson (AFWAL/FIG) for their support of this effort and valuable technical input throughout the project.

A

TABLE OF CONTENTS

LIST OF ILLUSTRATIONS

LIST OF TABLES

SECTION I

INTRODUCTION AND SUMMARY

OBJECTIVES OF THE RESEARCH

With the advent of active control technology (ACT) and control configured vehicles, the use of specifications on the rigid body modes of an aircraft for flight control design becomes unacceptable. Reducing structural weight by employing active flutter suppression or stability augmentation, and enhancing maneuverability by direct-lift and side-force control surfaces are some of the topics of current flight vehicle research. Such vehicles, however, intrinsically involve dynamics of higher order than the rigid body modes, and these dynamics have been shown to significantly alter piloted vehicle performance as well as subjective pilot ratings of the systems. The inclusion of such additional dynamics in the determination of the acceptable open-loop systems characteristics so drastically increases the dimensions of the problem as to render this approach, impractical. Furthermore, this is attacking the problem "upside down and backwards."

The ultimate design objective is to maximize the performance of the man-vehicle system. The most logical approach would seem to be to develop and apply systems analysis methods based on closed-loop, task-oriented design techniques - representing the man in the system appropriately as a dynamical decision and control element. Attacking the problem this way naturally leads to "optimal control configured vehicles" and forces one to ask the right questions along the way. For example, we naturally address the questions of what physical parameters the pilot is monitoring and attempting to regulate in specific piloting tasks. Only after answering

such fundamental questions can one make an intelligent design decision with regard to factors that would affect these relevant physical parameters.

The objective of this research activity then was to explore the utility of multi-variable control techniques for piloted-flight-vehicle control synthesis, with the above factors in mind, by application to a specific piloting task.

The methodology, developed previously, employs an optimal multivariable control model (OCM) of the pilot, specifically includes the pilot's mission objectives for control synthesis, and simultaneously determines the pilot's analytical representation (or model) and augmentation control law. As a result, the method is intended to be well suited for high-order dynamical systems, inherently reflect the cooperative structure of the pilot and flight control system, and at the same time include the pilot's ability to adapt to the controlled system dynamics. The original development of this method is reported in Reference 1, and the approach could be considered an optimal control version of a control design approach utilizing Anderson, "paper pilot".[2]

SUMMARY OF RESULTS

The piloting task addressed throughout the study was air-to-air tracking. The initial phase involved the analysis and vehicle augmentation for single axis pitch tracking, the system dynamics including active heads-up display dynamics as well as those of the vehicle rigid body. Fixed-base simulation data obtained elsewhere[3] were used to determine the pilot model parameters, specifically, the objective function and those determining the observation and neuromotor noise characteristics. It was significant that a unique objective function was found in the study cited for the task

in question, over a variety of vehicle dynamics. Such an assumption would be necessary for use in augmentation synthesis.

By parametrically varying the level of optimal-control augmentation, not only rms tracking-error performance improvements were predicted, but trends in desirable system dynamics were obtained. These trends were depicted as open-loop as well as piloted closed-loop system root loci and the agreement was noted between these loci and the asymptotic behavior of linear quadratic-optimally-controlled systems. Significant in this regard is the appearance of "pseudo zeros" or transmission zeros in the results and their importance in interpreting these results. Specifically, p of the augmented system roots tend to move toward the transmission zeros, and the n-p remaining roots ultimately approach a Butterworth-type pattern, where n is the order of the system and p is the number of transmission zeros.

The dynamics of the displays were found to affect the "optimal" vehicle characteristics. Agreement was found between the results for the less "active" of the two sights and previous results obtained with a fixed sight (and no display dynamics). However, with the more dynamic of the two displays, a different set of desired vehicle roots were obtained. Clearly then the complete system's dynamics must be considered, not just the rigid-body eigenvalues. Furthermore, the numerator dynamics (which include the display dynamics) were found to affect the desired system characteristics (e.g., handling qualities).

With the augmentation determined, the pilot model was then used to predict rms performance (e.g., tracking errors) as well as pilot and vehicle describing function frequency response. This analysis indicated

the potential for significant reduction in tracking error and pilot workload, with an anticipated improvement in pilot rating.

The second phase of the study involved a similar analysis of air-to-air tracking in a highly-banked turning flight condition. As such, it involved pilot/vehicle analysis of a flight condition in which the longitudinal and lateral-directional axis were not independent, but involved unsymmetrical cross coupling. Consequently, a significant amount of pilot-modeling activity was necessary as no multi-axis pilot models have been developed and documented.

To accomplish this modeling activity, results from a large-amplitude motion simulation (the Air Force LAMARS facility at Wright-Patterson AFB, Ohio) were compared to predicted rms performance. It was determined that in addition to tracking error and displayed target lead angle, the weighted outputs in the single-axis pilot objective function, the pilot was also attempting to minimize lateral acceleration and relative bank angle between the attacker and target. Hence, the pilot's vector of observations as well as the objective function weights were modified appropriately.

The use of this pilot-modeling approach for tracking a target not undergoing random maneuvers was another unique result of this phase. Without a random forcing function (or process noise) the pilot's observation and motor noise are the only source of errors. Since this was actually the situation simulated, the modeling proceeded appropriately. The solution involved selecting the variances of the additive motor noises yielding the best match of statistical results (i.e., rms performance), and a result of this modeling task is the noise-to-signal ratio for the motor noises.

This multi-axis pilot model having been established, the multi-variable augmentation synthesis followed directly. Again, a family of

full-state feedback control laws were synthesized with the pilot-optimal control formulation, and the open- and closed-loop root loci used to depict the trends in system dynamics (in terms of the eigenvalues). The longitudinal results were found to agree with the single-axis results using the same display dynamics, and were explainable in terms of the asymptotic behavior of optimally controlled systems.

The more complex lateral directional axis was also found to yield results consistent with the asymptotic properties. The dutch-roll mode was augmented to yield significantly higher frequency and damping, ultimately approaching a Butterworth configuration, while the spiral and roll subsidence were coupled to form a complex, stable roll/spiral mode.

It is significant, in closing, that the pilot/vehicle analysis and augmentation results all point to the high relative importance and complexity of the lateral directional axis. The parameters associated with this axis required much higher attentional allocation, as determined by the pilot model, and the dynamics were highly modified via augmentation. Yet this axis has received far less attention in the literature and even less experimental activity is apparant. Much further work is therefore called for in our opinion.

ORGANIZATION OF THE REPORT

The following section (Section II) includes the complete analysis and results from the first phase of the study, that involved with single-axis pitch tracking. The multi-axis pilot/vehicle analysis and augmentation is reported in Section III.

A significant amount of the effort of the project was devoted to modeling the vehicle, display, and target kinematics and dynamics, these results are documented in Appendices A through D. The matrices defining the linear state variable model of the multi-axis tracking problem is given in Appendix E.

Finally, a management summary, citing publications, students involved, and interactions with Air Force Laboratory personnel appears in Appendix F.

SECTION II

PITCH TRACKING ANALYSIS AND AUGMENTATION

The problem to be addressed is the analysis and augmentations of the plant dynamics in an (air-to-air pitch) tracking task. The higher-order system dynamics actually include linearized flight vehicle rigid-body and actuator dynamics as well as the display dynamics of two lead-computing sights. In each of the cases considered, the vehicle flight condition, and therefore rigid-body dynamics, remain unchanged. However, the sight dynamics vary considerably between cases with different sight types and different tracking ranges.

The vehicle and one of the sights was identical to one of the cases addressed experimentally, as well as analytically (via the OCM), by Harvey.[3] In his investigation, Harvey used fixed-base simulation data to infer the pilot's objective function in this task. A unique objective function was found to yield extremely good correlation (in terms of rms statistics) between analytical and experimental results over a wide range of system dynamics. It is therefore assumed in our work here, that this same objective function is invariant with the system dynamics, and is used in all cases considered.

The objectives of this part of the investigation then include not only the estimation of the performance improvement attainable with augmentation, but also, and perhaps more important, the determination of the most desirable plant or controlled element dynamics. By parametrically varying the level of augmentation, we are able not only to establish trends in the desirable plant characteristics with varying high-order plant characteristics. Finally, the results so obtained are compared to those of Hollis,[4] who used simple pitch-rate and

plunge-acceleration feedback along with Anderson's paper pilot to determine optimum vehicle dynamics for pitch tracking with a fixed sight (with no display dynamics).

THE SYSTEM MODELS

The vehicle dynamics are the linearized short-period approximation for a typical fighter aircraft in level flight at 15,000 ft. altitude, Mach = 0.9 (V = 952 ft/sec), and the specifics are presented in Table 1. Also, to aid in the

TABLE 1

VEHICLE MATH MODEL

$$\dot{\alpha} = Z_\alpha \alpha + q + Z_\delta \delta_E$$

$$\dot{\theta} = q$$

$$\dot{q} = (M_\alpha + M_{\dot{\alpha}} Z_\alpha)\alpha + (M_q + M_{\dot{\alpha}})q + (M_\delta + M_{\dot{\alpha}} Z_\delta)\delta_E$$

$$\dot{\delta}_E = -\frac{1}{\tau_a}\delta_E + 16\delta_{stick}$$

$Z_\alpha = -983.\ (ft/sec^2)$ $M_\alpha = -10.4\ (rad/sec^2)$

$Z_\delta = -90.5\ (ft/sec^2)$ $M_{\dot{\alpha}} = -0.344\ (rad/sec)$

$\tau_a = .05\ sec$ $M_q = -0.738\ (rad/sec)$

$\zeta_{SP} = 0.32;\ \omega_{SP} = 3.35\ (rad/sec)$ $M_\delta = -37.1\ (rad/sec^2)$

interpretation of results, we will consider augmenting the simple, second-order plant $(\theta(s)/\delta_{st}(s) = K/s^2)$.

The schematics of the displays are shown in Fig. 1. The tracking task of course involves the desire to minimize the tracking error ϵ, where for the simple K/S^2 plant

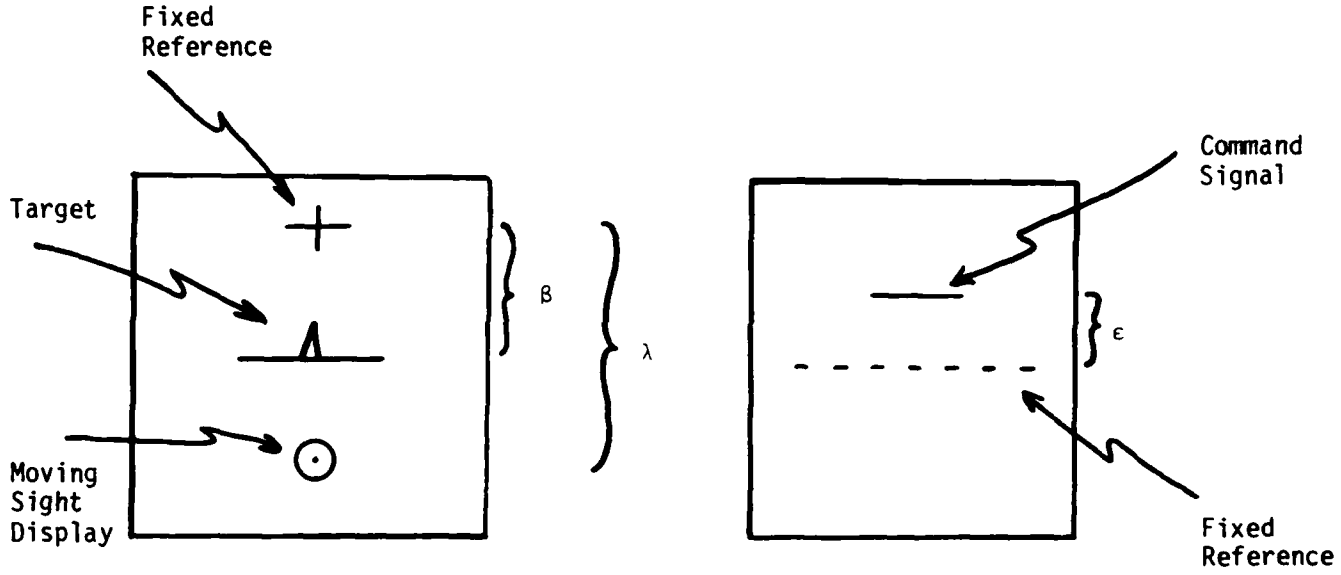

Fig. 1 Display Schematics

$$\varepsilon = \theta - \theta_c$$

For the pitch tracking task

$$\varepsilon = \lambda - \beta$$

where β, the relative line-of-sight angle is governed by the relations

$$\dot{\beta} = q - \frac{V}{D}(\gamma_T - \theta + \alpha)$$

$$\dot{\gamma}_T = -\frac{1}{V} a_T$$

Note for this display, the fixed reference mark represents the weapon line and the sight (reticle and pipper) is dynamic (moves in display).

For the high-order pitch-tracking task, the displayed variable, or lead angle λ, includes the lead required for velocities and accelerations, as well as a ballistic "jump" correction. The governing linearized equation of an ideal sight is (from Appendix B)

$$\lambda = T_f(\dot{\theta} - \dot{\beta}) - \frac{T^2_f}{2D} a_T - .038 \frac{VT_f}{D} \alpha \qquad (1)$$

This relation implies that the line-of-sight rate $\dot{\beta}$ and the target's normal acceleration a_T, are available for lead-angle calculation, and therefore represents an idealized sight. A second lead-angle equation representing an actual typical sight is given as (from Appendix B)

$$\dot{\lambda} = -\frac{1}{T_f} \lambda - \left(\frac{Z_\alpha T_f}{2D} + .038 \frac{V}{D}\right) \alpha + \dot{\theta} \qquad (2)$$

This relation is obtained from the above by assuming the line-of-sight rate $\dot{\beta}$, may be approximated by the lead-angle rate $\dot{\lambda}$, and the target acceleration is approximately equal to the attacker's, or $a_T \simeq Z_\alpha \alpha$. Note that since the actual sight (Eqn. 2) depends entirely on the attacker's variables (α,θ, etc), it is much more sensitive to pilot stick input than the ideal sight. Also note the

sight dynamics are clearly a function of tracking range. Two tracking ranges were considered, D = 1000 ft. and D = 3000 ft, associated with two projectile times of flight, T_f = 0.33 sec. and T_f = 1.30 sec, respectively. The process driving noise for the pitch tracking case is the target normal acceleration generated by filtered white noise where

$$\dot{a}_T = -.33a_T + n$$

$$\dot{n} = -0.33n + w(t)$$

and the white noise intensity is selected to yield chosen levels of target accelerations. The driving noise for the K/s^2 plant is simply the commanded variable θ_c, generated by filtered white noise where

$$\ddot{\theta}_c + a\dot{\theta}_c + b\theta_c = w(t)$$

For comparison purposes, the transfer functions for the three systems are given in Table 2. The numerator coefficients N_1 - N_4 and M_1 - M_4 are functions of vehicle and sight characteristics, and therefore depend on tracking range or, equivalently, T_f. On the other hand, except for the sight time constant T_f in the typical-sight case, the denominator is a function of vehicle characteristics alone.

The optimal-control model (OCM) of the pilot[5] assumes that the well-trained, well-motivated human operator chooses his control inputs $\bar{u}_p$, subject to human limitations, such that following objective function is minimized

$$J_p = E\{\lim_{T\to\infty} \frac{1}{T} \int_0^T (\bar{y}'Q\bar{y} + \bar{u}_p'R\bar{u}_p + \dot{\bar{u}}_p'G\dot{\bar{u}}_p)dt\} \qquad (3)$$

and G is selected to obtain a chosen neuromuscular lag time constant τ_N. The pilot's input is then expressed in the scalar case as

$$\tau_N\dot{u}_p = -K_x\hat{\bar{x}} - u_p$$

The selected parameters of the model in this investigation are given in Table 3 , and are consistent with those in Harvey's investigation of this task. (Note that nominal values of model parameters have been chosen which do not reflect the pilot's acceleration environment. This was done to be consistent with fixed-base simulation results.)

TABLE 2

TRANSFER FUNCTION COMPARISON

Second order plant:

$$\frac{\varepsilon(s)}{\delta_{st}(s)} = \frac{11.7}{s^2}$$

Ideal sight display:

$$\frac{\varepsilon(s)}{\delta_{st}(s)} = \frac{K(N_1 s^3 + N_2 s^2 + N_3 s + N_4)}{s^2(\tau_a s + 1)(s^2 + 2\zeta_{sp}\omega_{sp} s + \omega_{sp}^2)}$$

Typical sight display:

$$\frac{\varepsilon(s)}{\delta_{st}(s)} = \frac{K(M_1 s^3 + M_2 s^2 + M_3 s + M_4)}{s^2(T_f s + 1)(\tau_a s + 1)(s^2 + 2\zeta_{sp}\omega_{sp} s + \omega_{sp}^2)}$$

$$K = -16\ \tau_a / D$$

$$N_1 = -.962 Z_\delta T_f$$

$$N_2 = (\frac{D}{V} + T_f)(VM_\delta + Z_\delta M_{\dot{\alpha}}) - Z_\delta$$

$$N_3 = Z_\delta(M_q + M_{\dot{\alpha}}) + (\frac{D}{V} + T_f)(M_\alpha Z_\delta - Z_\alpha M_\delta)$$

$$N_4 = M_\alpha Z_\delta - Z_\alpha M_\delta$$

$$M_1 = Z_\delta T_f(\frac{Z_\alpha D}{2V^2} - .962)$$

$$M_2 = N_2 + T_f(\frac{Z_\alpha D}{2V^2} - .962)(VM_\delta - M_q Z_\delta)$$

$$M_3 = N_3;\ M_4 = N_4$$

TABLE 3

PILOT MODEL PARAMETERS

Observation delay, $\tau = 0.2$ sec

Neuromuscular time constant, $\tau_N = 0.1$ sec

Observed variables, $\bar{y}' = [\varepsilon, \dot{\varepsilon}, \lambda, \dot{\lambda},]$

Cost function weightings, $Q_{y_{ii}} = [16,1,0,4]$

$R_u = 0$

Full attentional allocation

Observation thresholds, $T_\varepsilon = T_\lambda = 0.65$ deg

$T_{\dot{\varepsilon}} = T_{\dot{\lambda}} = 1.3$ deg/sec

Observation noise variance $V_{y_i} = \pi\rho_y\sigma^2_{y_i}$, $\rho_y = .01$

Motor noise variance, $V_{u_p} = \pi\rho_u\sigma^2_{u_p}$, $\rho_u = .001$

Shown in Table 4 is the predicted (rms) performance using this OCM as compared with Harvey's (fixed-base simulator) experimental results for the typical sight display. Also shown is the predicted performance for the idealized sight for reference.

SYSTEM AUGMENTATION

With the above system models, we represent the system, including the pilot's control input as well as the augmentation input, by the relation

$$\dot{\bar{x}} = A\bar{x} + B\bar{u}_p + B\bar{u}_{aug} + \bar{w}$$

where u_{aug} is an equivalent stick input, a scalar, in this case. As shown previously,[1] if $\bar{u}_{aug}$ is chosen to minimize the objective function

TABLE 4

PERFORMANCE COMPARISON

D = 1000 ft σ_T = 3.5 g	Parameter (rms) ε(deg)	λ(deg)	q(deg/sec)	δ_E(deg)
Experiment	2.1	2.9	8.0	2.1
Analytical (Typical sight)	2.3	2.9	8.7	2.1
Analytical (Ideal sight)	1.6	2.6	7.9	2.0
D = 1000 ft σ_T = 5 g				
Experiment	2.7	4.0	11.2	3.0
Analytical (Typical sight)	3.0	4.2	12.1	3.0
Analytical (Ideal sight)	1.9	3.7	11.0	2.9
D = 3000 ft σ_T = 3.5 g				
Experiment	2.4	8.7	6.4	1.8
Analytical (Typical sight)	2.3	10.1	7.3	1.8
Analytical (Ideal sight)	1.1	9.7	6.0	1.6
D = 3000 ft σ_T = 5 g				
Experiment	2.7	12.1	9.2	2.4
Analytical (Typical sight)	2.7	14.2	10.2	2.5
Analytical (Ideal sight)	1.4	13.8	8.5	2.3

$$J_{aug} = J_p + E\{\lim_{T\to\infty} \frac{1}{T} \int_0^T \bar{u}'_{aug} F \bar{u}_{aug}\, dt\} \qquad (4)$$

where J_p is given in Eqn. 3 , the relation for the augmentation input is

$$\bar{u}_{aug} = -F^{-1}B'K_{A_1}\bar{x} - F^{-1}B'K_{A_2}\bar{u}_p$$

or

$$\bar{u}_{aug} = -K_x\bar{x} - K_u\bar{u}_p$$

(The matrices K_{A1} and K_{A2} are obtained, as discussed in Reference 1, by simultaneously solving two coupled Riccati equations, one yielding the augmentation gains, and one yielding the pilot's gains.).

The result, of course, is the pilot controlling the augmented system, which is now described by

$$\dot{\bar{x}} = (A - BK_x)\bar{x} + B(I - K_u)\bar{u}_p + \bar{w}$$

or

$$\dot{\bar{x}} = A_p\bar{x} + B_p\bar{u}_p + \bar{w}$$

Second-Order Plant

Let us initially consider the effects of pilot optimal augmentation of the second order plant (for which we may define $\bar{x}' = (\theta_c, \dot{\theta}_c, \theta, \dot{\theta})$ and $y' = (\epsilon, \dot{\epsilon})$). Shown in Fig. 2 is the augmented open-loop and pilot closed-loop root locus obtained via optimal augmentation for various u_{aug} objective-function weights, or F in Eqn. 4 . (A-E indicate open- and closed-loop cases with increasing augmentation.) Note the shape of the augmented (open-loop) system root locus as well as that of the pilot closed-loop system corresponds to the known[6] asymptotic behavior of the closed-loop roots of a linear optimally controlled single-input, single-output system. In this case, the root locus assumes a Butterworth configuration of order two. (This results from two open-loop plant poles and no zeros. Except the pilot closed-loop poles include a third introduced via the pilots neuromuscular lag.)

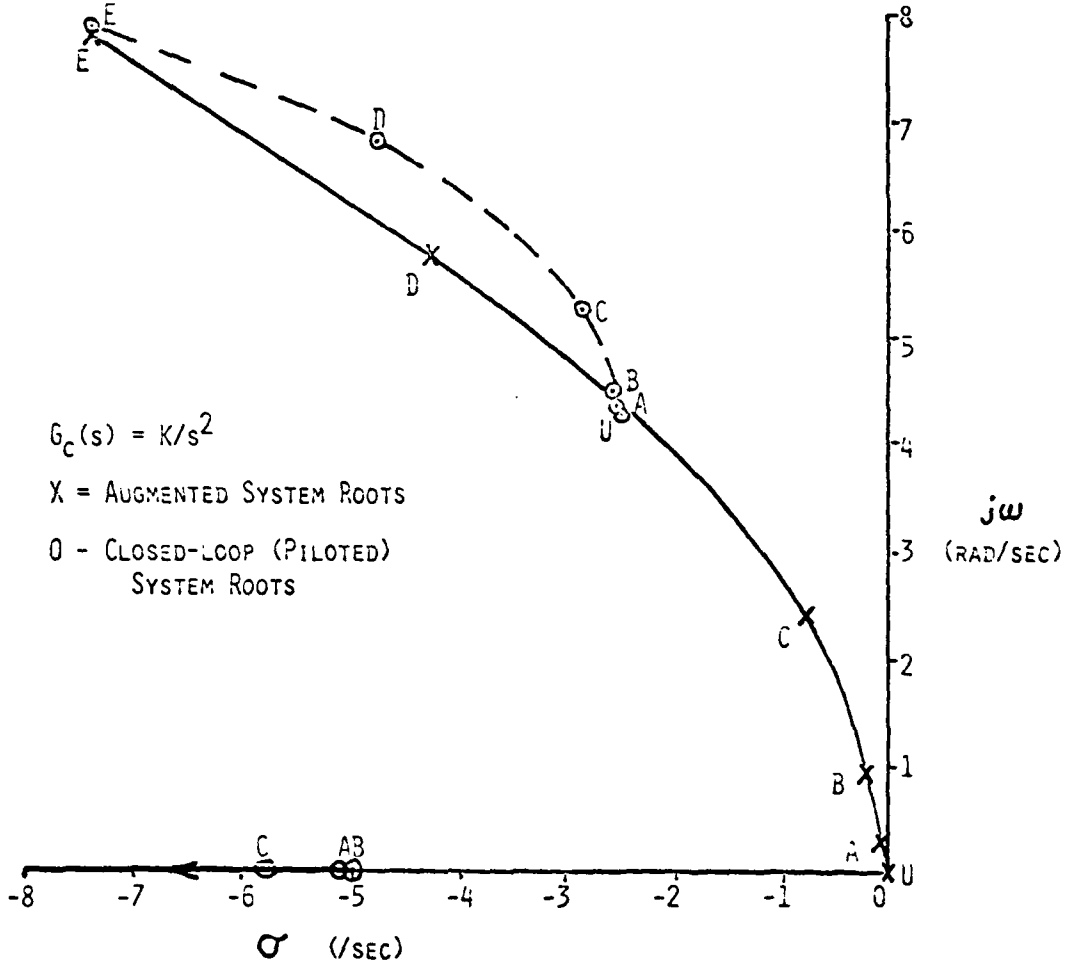

Fig. 2 Root Locus-Second Order Plant

The distance between open-loop and closed-loop eigenvalues is a maximum for no augmentation (i.e. $F \to \infty$), while the open-loop and closed-loop poles coalesce for increasing augmentation, eventually eliminating the pilot compensation, and the system monotoically approaches a pure automatically controlled system.

To aid in further interpretation of these results, consider the human operator describing function in a compensatory task to be approximated by

$$H(s) = \frac{K_p e^{-\tau s}(T_L s + 1)}{(\tau_N s + 1)}$$

or a gain, low-frequency lead, effective delay, and neuromuscular lag. Our augmented or unaugmented second-order plants may be described in general by the transfer function

$$G(s) = \frac{K}{s^2 + 2\zeta\omega s + \omega^2}$$

The piloted closed-loop denominator now becomes (ignoring the delay)

$$s^3 + (\frac{1}{\tau_N} + 2\zeta\omega)s^2 + [\omega^2 + \frac{1}{\tau_N}(2\zeta\omega + KK_pT_L)]s + \frac{1}{\tau_N}(\omega^2 + KK_p)$$

If we write this closed-loop denominator as

$$(T_c s + 1)(s^2 + 2\zeta_c\omega_c s + \omega_c^2)$$

or

$$s^3 + (\frac{1}{T_c} + 2\zeta_c\omega_c)s^2 + (\omega_c^2 + \frac{1}{T_c} 2\zeta_c\omega_c)s + \frac{1}{T_c}\omega_c^2$$

we see that the pilot's gain K_p is related to the difference between open- and closed-loop frequencies by the relation

$$KK_p = \frac{\tau_N}{T_c}\omega_c^2 - \omega^2$$

Therefore, the pilot's gain tends to be proportional to the difference between the squares of closed- and open-loop natural frequencies, or equivalently, the squares of distances of the poles from the origin.

Also, the pilot's lead T_L, is related to the open- and closed-loop parameters by the relation

$$T_L = \frac{\tau_N[(\omega_c^2 - \omega^2) + 2(\zeta_c\omega_c/T_c - \zeta\omega/\tau_N)]}{(\frac{\tau_N}{T_c}\ \omega_c^2 - \omega^2)}$$

Therefore, the pilot's lead would tend to increase with increasing $\Delta(\zeta\omega)/\Delta\omega^2$ between open- and closed-loop eigenvalues. With these observations, we are able to qualitiatively relate the trends from the root locus (Fig. 2) to the parameters in the classical human operator describing function.

In the case of higher order systems, however, the pilot describing function may not be well approximated by the simpler forms, and the relationships between the root locus characteristics and the predicted human describing function parameters are much more complex and difficult to express quantitatively. Still, the effects of augmentation, and of the pilot's gains are depicted in the root loci, and the difference between the open- and closed-loop roots indicate at least qualitatively the required level of human equalization involved. And finally, the augmented (open-loop) system root locus yields important information about the desirable trends in the systems dynamics.

Ideal Sight Display

Consider now, the optimal augmentation of the air-to-air tracking task with the system including the ideal sight display (lead angle obtained from Eqn. 1). Again, with descreasing augmentation-control-input weight (F in. Eqn. 4), we generate a family of augmented systems. The open- and closed-

eigenvalues are shown in Fig. 3 .

The open-loop roots include, the unaugmented case, the two roots at the origin, the vehicle short-period roots, and the actuator root at -20(rad/sec.)

For the piloted closed-loop system, still unaugmented, the roots include a low-frequency pair, a high-frequency pair, and two real roots, one at -3.7 rad/sec and one (not shown for clarity) at -20 rad/sec.

As the level of augmentation is increased, as indicated by cases A-C, the frequency and damping of the vehicle short period mode is increased, and the two poles originally at the origin move toward the piloted closed-loop low-frequency pair due to the closure of the tracking loop (i.e., feedback of ε and $\dot{\varepsilon}$). With the pilot closing the loop on the augmented systems a unique pair of high frequency roots are associated with each level of augmentation, and this pair appears to follow a Butterworth pattern. However, for the levels of augmentation considered, the two real closed-loop roots (at approximately -20 and -3.7 rad/sec) are relatively insensitive to augmentation level. Also, the low-frequency pair (at about $-.7 \pm .7j$) are invariant with augmentation. This pair also corresponds closely to a pair of plant zeros.

This behavior is consistent with the asymptotic properties of linear optimally controlled system roots cited previously. For single-input, single-output systems p of the roots tend toward the p open-loop zeros (in the left half plane), and the remaining roots assume a Butterworth configuration of order n-p. Furthermore, the systems with input and output vectors of equal dimension (i.e., systems with square transfer-function matrices), p of the closed-loop roots tend to the p "zeros" of the determinant of the transfer-function matrix. Although, the transfer-function matrix is not square in this

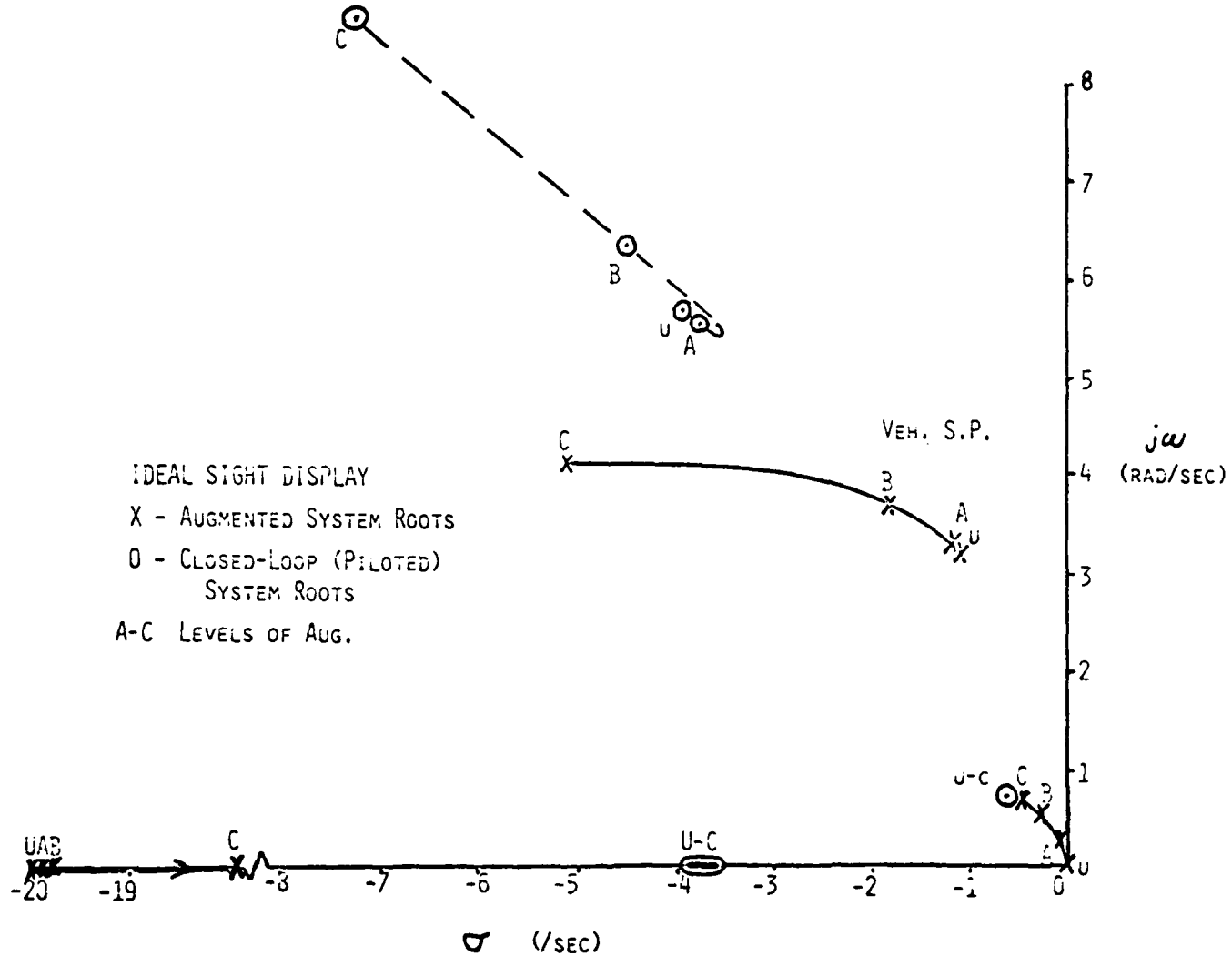

Fig. 3 Root Locus-Ideal Sight Display

case, the invariance of any closed-loop roots may still be explained in terms of the above properties and the existence of system "pseudo zeros."

Shown in Fig. 4 is the comparison of these (vehicle short period) results with those of Hollis. In his analysis, Hollis determined the vehicle augmentation yielding the best pilot rating via the "paper-pilot". Pitch rate and plunge acceleration were used for augmenting only the vehicle with a fixed sight (with no display dynamics). It is seen that the results agree with the trend determined by Hollis' consideration of several sets of vehicle dynamics. In all cases, the "optimal" augmentation increased the frequency and damping of this vehicle mode. This trend, as noted by Hollis, also agrees with the military specifications on flying qualities. (As we shall see later, this is not the case for the other sight display.)

The predicted improvement in (rms) tracking accuracy for the ideal sight is shown in Table 5, along with the rms statistics on stick deflection and rate of deflection (i.e., physical workload). Recall that the stick deflection was not considered penalized in the pilot's objective function, hence little reduction in this parameter is obtained through augmentation. However, rms stick rate is significantly reduced.

Finally, Table 6 lists the optimum full-state feedback gains in this idealized case, for each level of augmentation.

For this sight display, increasing the tracking range D, from 1000 ft. to 3000 ft. changed the results very slightly. The feedback gains varied approximately 15 percent and the augmented and piloted system root loci were almost identical to that in Fig. 3. The position of the invariant, low-frequency piloted-system roots did change from $-.7 \pm .7j$ to -.3 and -1.2 rad/sec, but

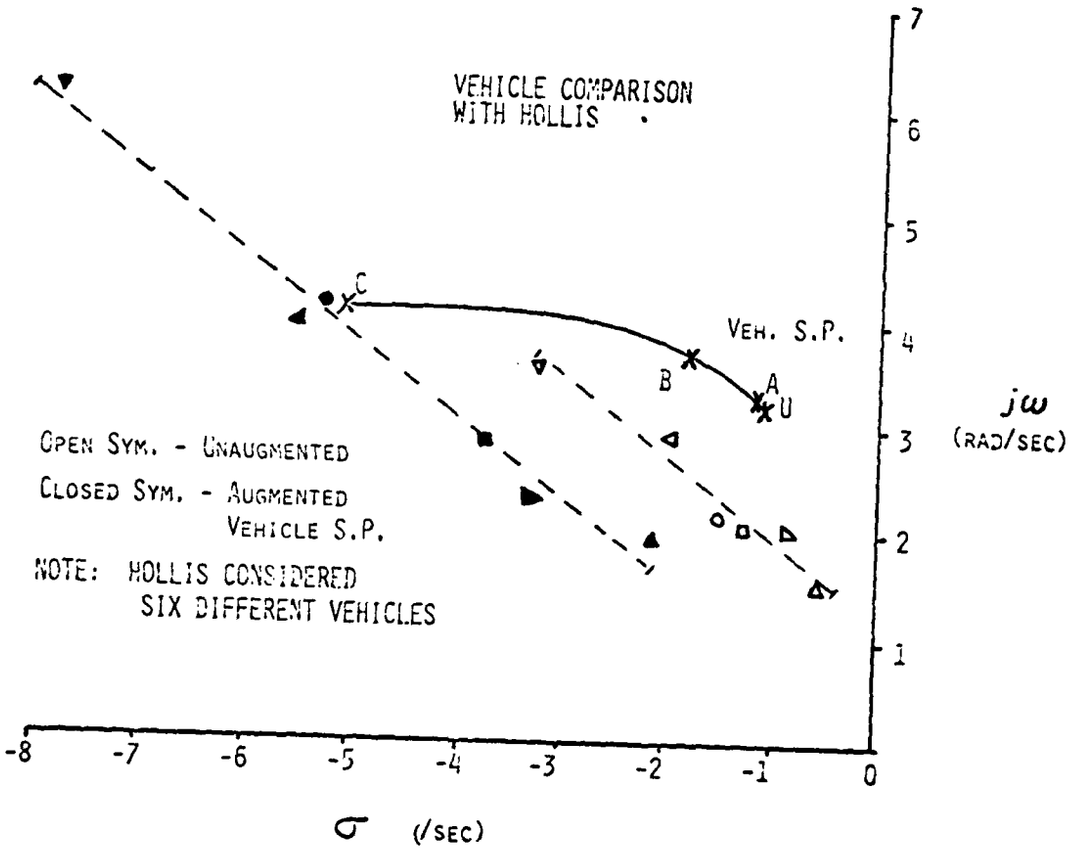

Fig. 4 Vehicle Dynamics Comparison

TABLE 5

AUGMENTED PERFORMANCE (rms)

	Unaugmented	Level A	Level B	Level C
Error, ϵ(deg)	1.92	1.71	0.95	0.35
Deflection, δ(deg)	3.61	3.55	3.50	3.55
Rate, $\dot{\delta}$(deg/sec)	7.16	6.25	5.39	4.87

σ_{aT} = 5 g's, D = 1000 ft.

TABLE 6

OPTIMUM GAINS - IDEAL SIGHT DISPLAY

Augmentation Level	K_n	K_{aT}	$K_{\gamma T}$	K_β	K_α	K_Θ	K_q	K_{δ_E}	$K_{\delta_{st}}$
Level A	$-.113\times10^{-5}$	$-.735\times10^{-5}$	.021	.030	.030	-.051	-.011	.017	.029
Level B	$-.725\times10^{-5}$	$-.492\times10^{-4}$	.144	.213	.189	-.357	-.072	.111	.154
Level C	$-.267\times10^{-4}$	$-.206\times10^{-3}$	.632	.995	.734	-1.63	-.314	.432	.383

the augmentation moved the poles at the origin toward those roots as in the 1000 ft. case.

Typical Sight Display

Considering now the system with the more typical display dynamics (lead angle computed with Eqn. 2), the open- and closed-loop root loci are shown in Fig. 5. The unaugmented system roots in this case include those considered above, plus the lead-angle time constant T_f. Comparing these results with those in Fig. 3, we see an entirely different trend in the vehicle short-period roots! With the more sensitivity, or "active," sight display in this case, the optimum short period frequency remains relatively constant while the damping is increased. Recall that the results obtained by Hollis included no display dynamics, and that the results agreed with those obtained with the less active, ideal sight display. Additionally, the augmented short-period roots in the case considered here (Fig. 5) approach an invariant pair of piloted closed-loop eigenvalues, a trend not observed in the ideal-sight case.

The behavior of the roots near the origin is as observed previously, the augmentation closing the tracking loop and moving the plant poles at the origin toward the two invariant closed-loop eigenvalues. Also, the actuator and sight time constants move together, due to augmentation, and eventually become a high-frequency, complex pair. Finally, as before, a unique, high-frequency closed-loop pair is associated with each level of augmentation, and approaches a Butterworth pattern. A seventh closed-loop root at -20 rad/sec is the actuator root remaining, but is not shown for clarity.

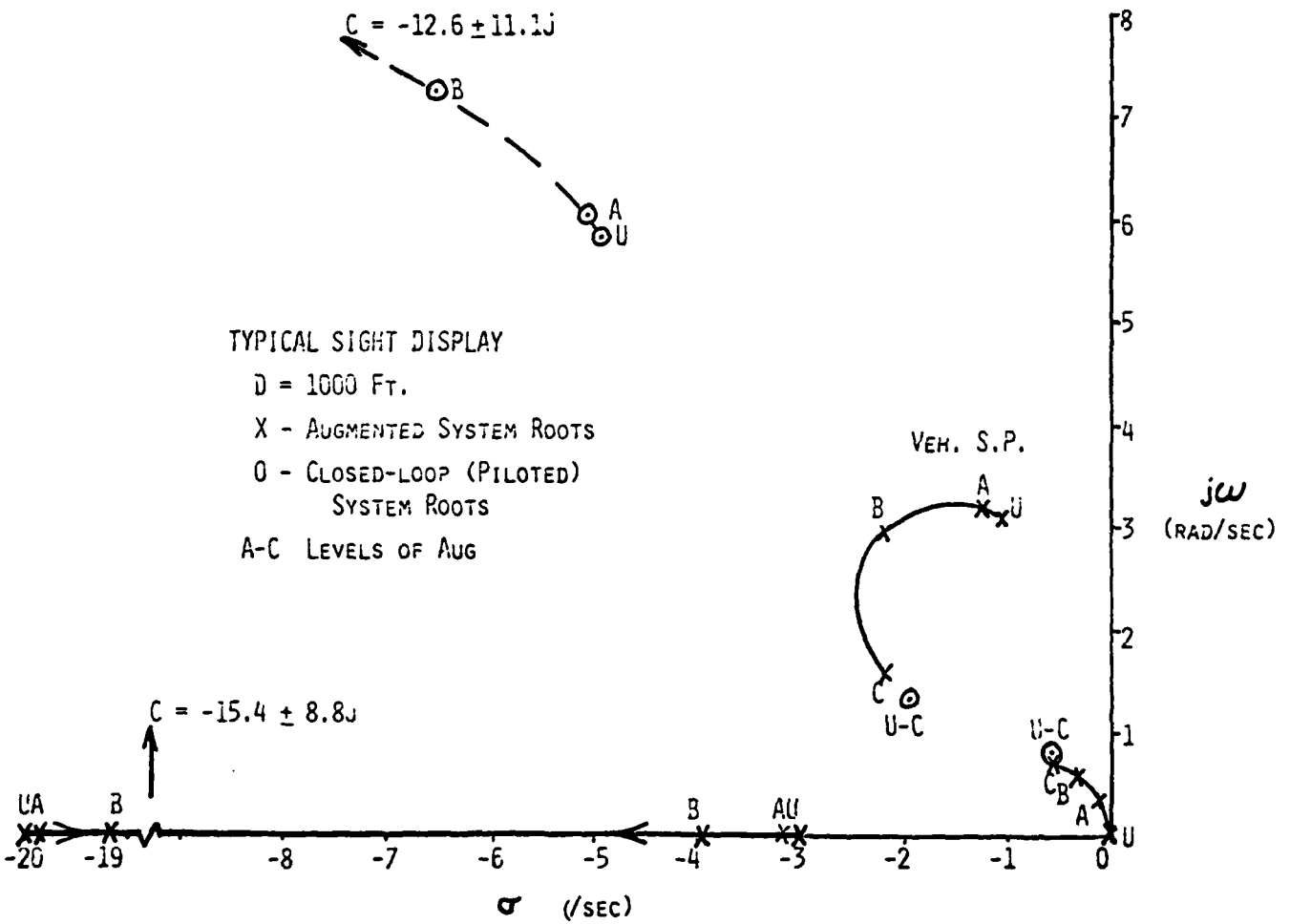

Fig. 5 Root Locus-Typical Sight (1000 ft)

Increasing the range to the target D from 1000, to 3000 ft. results in the root loci shown in Fig. 6. Now, not only do the plant zeros (and therefore the "pseudo-zeros") depend on D, but the sight time constant T_f is affected as well. As a result, this root locus is appreciably different from that in Fig. 5, particularly at the higher level of augmentation. Still present, however, are the four invariant closed-loop poles, two real and two complex in this case, and the family of complex closed-loop roots at the higher frequency. Note in this case, the migration of the sight time constant with augmentation toward the closed-loop at -.3 rad/sec, and the behavior of the augmented short-period roots for level C.

The effect of augmentation (level B, D = 1000 ft) on the system's frequency response (ε/δ) is depicted in Fig. 7. Closure of the tracking loop (via ε and $\dot{\varepsilon}$ feedback) eliminates the $1/s^2$ characteristic, at low frequency, while the increased damping of the short period mode (at $\omega \simeq 3.$ rad/sec) is evident. The effect of this level of augmentation on the predicted frequency response of the pilot is shown in Fig. 8. With augmentation, the pilot appears to increase his gain, as well as adding slightly more low frequency lag. Also, his required lead near $\omega = 3$ rad/sec. would appear to be decreased.

The pilot frequency response shown in this figure is that of an equivalent describing function formed from the transfer function matrix (H(s)) obtained from the optimal control pilot model. This equivalent describing function is analogous to the classical human describing function measured experimentally in a compensatory task, and is obtained from the relation

$$\left.\frac{\delta_{st}(s)}{\varepsilon(s)}\right|_{\text{Equiv.}} = \frac{\delta_{st}(s)}{\varepsilon(s)} + s\,\frac{\delta_{st}(s)}{\dot{\varepsilon}(s)} = h_{11}(s) + s h_{12}(s)$$

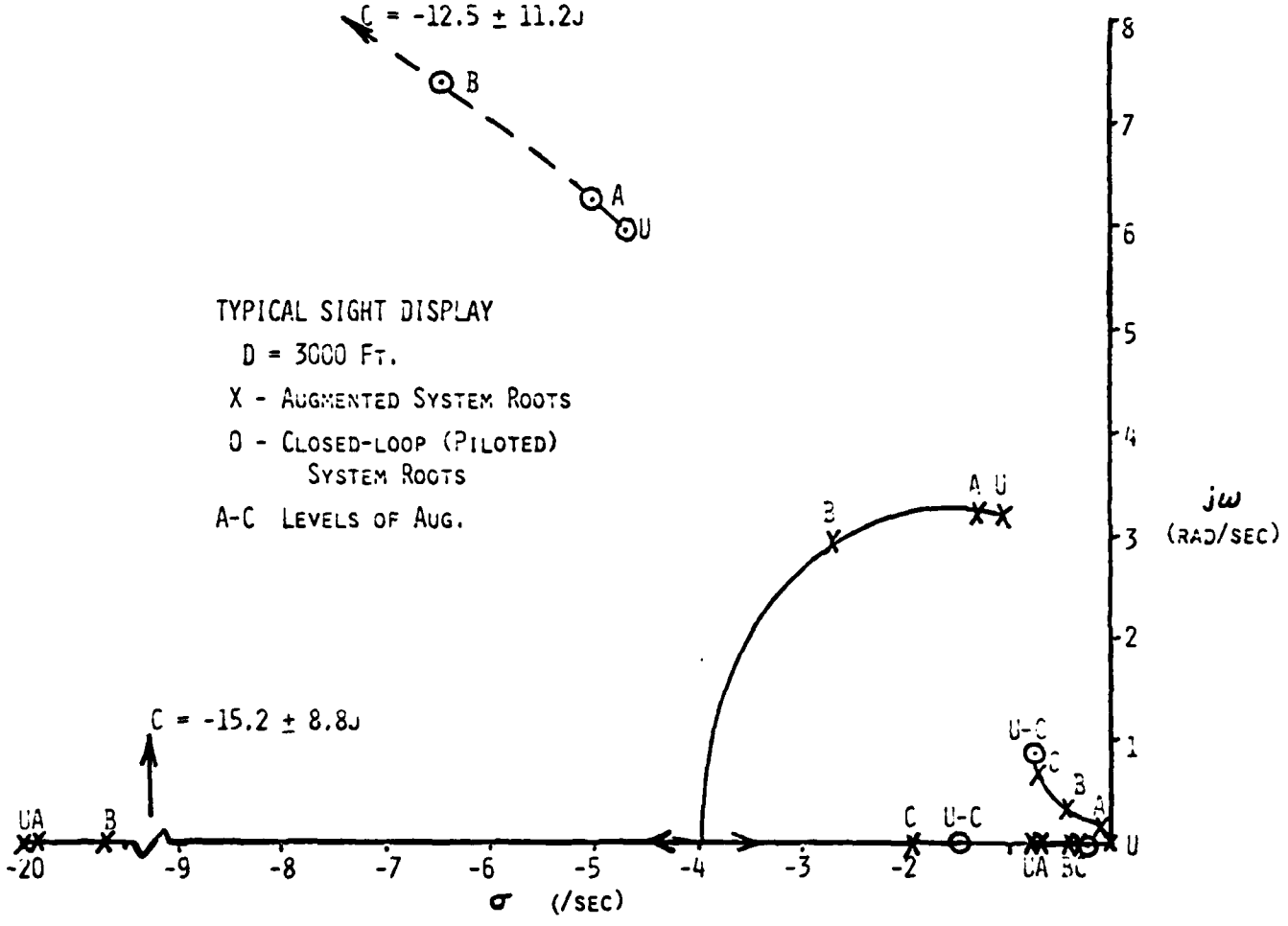

Fig. 6 Root Locus-Typical Sight (3000 ft)

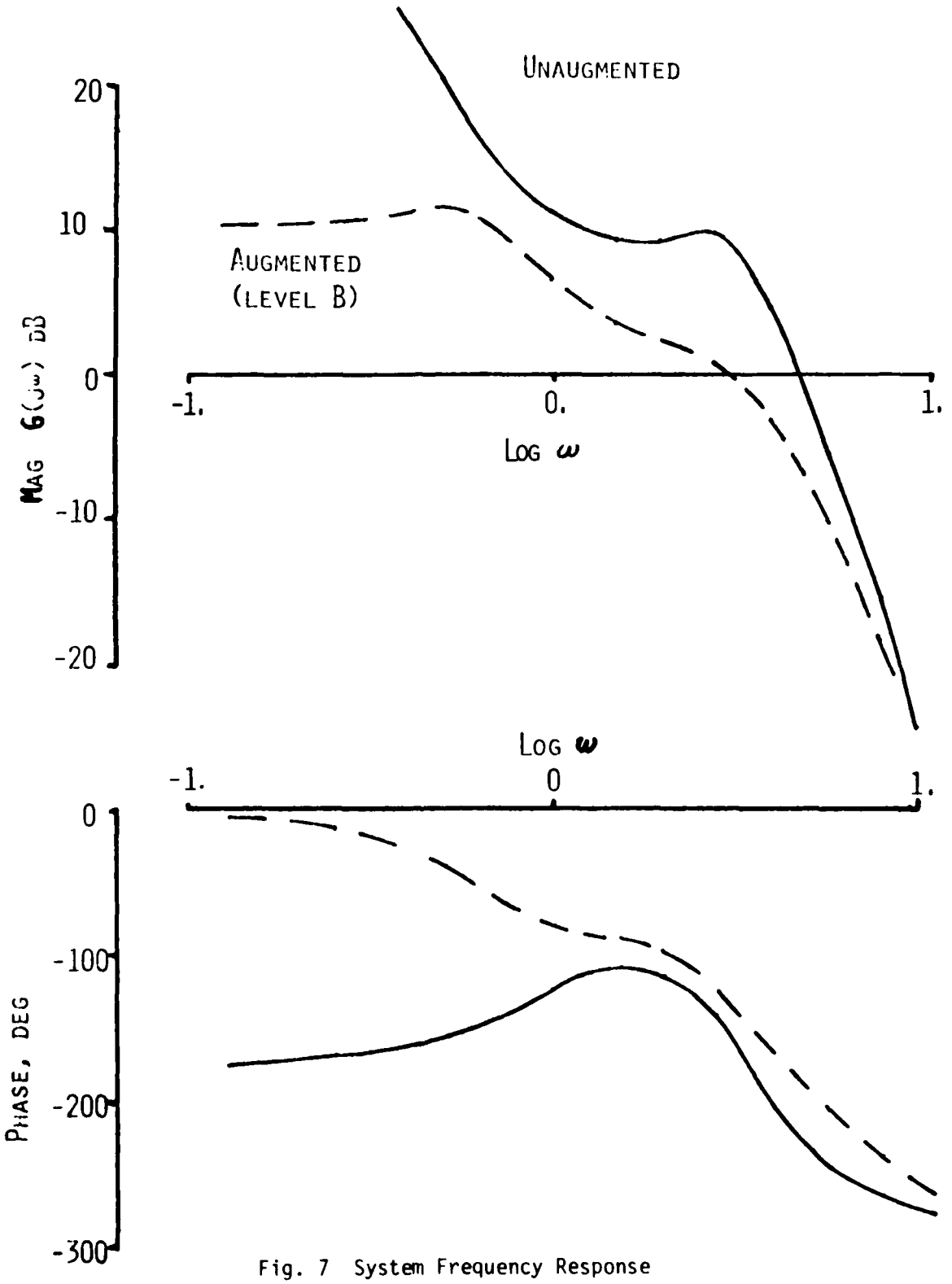

Fig. 7 System Frequency Response

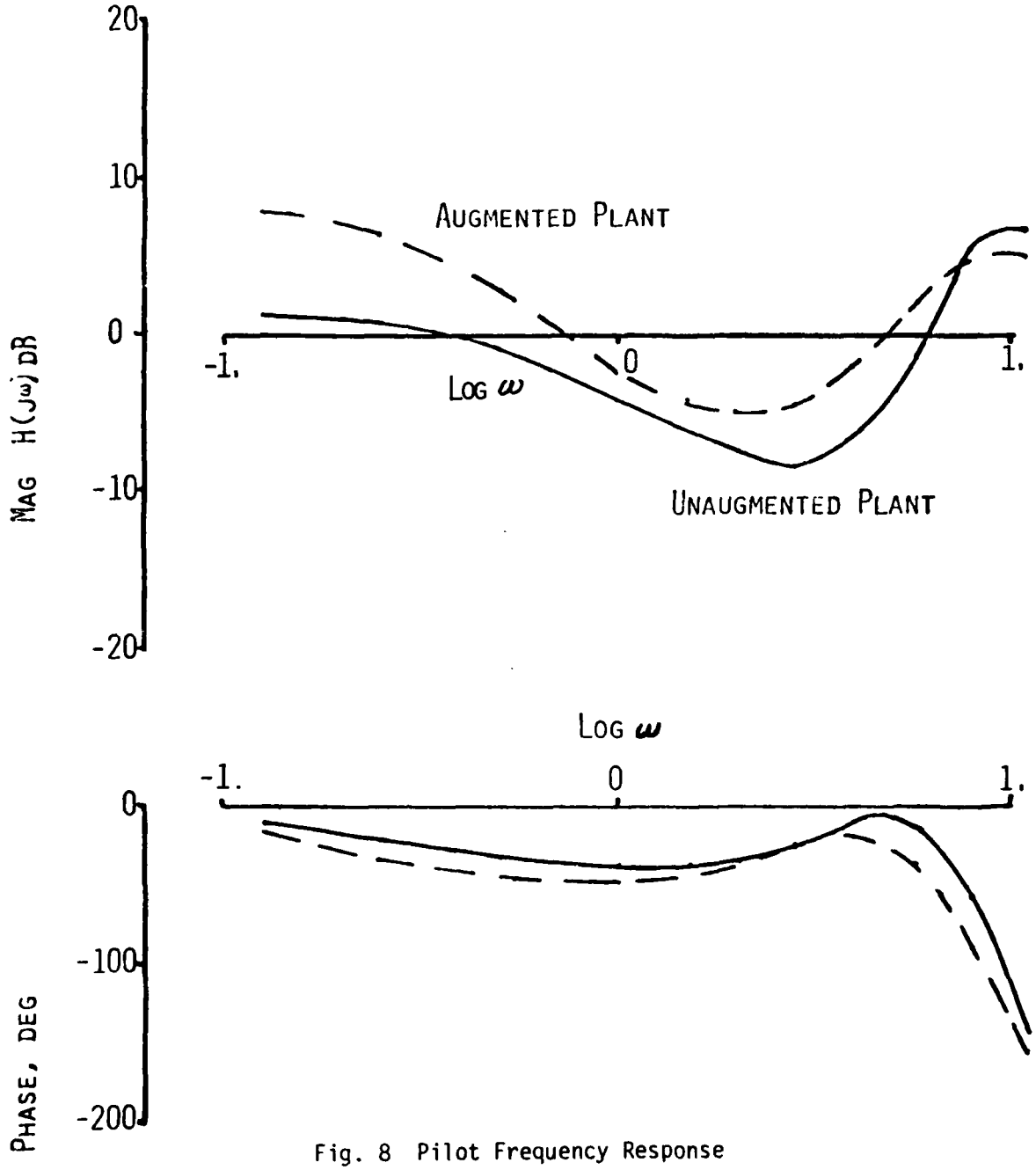

Fig. 8 Pilot Frequency Response

and where $\delta_{st}(s) = H(s)\ \bar{y}(s)$.

The effect of the augmentation on the predicted rms performance is shown in Table 7. The rms error ε, stick deflection and stick rate are given for D = 1000 ft., σ_{aT} = 5 g's. Here again we see a significant improvement in tracking error while the rms stick activity remains approximately constant with increased augmentation. As before, however, we note that stick activity was not penalized in the objective functions. The pilot stick rate is also reduced with augmentation.

The above improvements in tracking accuracy were obtained while the predicted elevator activity actually decreased slightly with increased augmentation (2.96 deg-rms unaugmented to 2.81 deg-rms for level C). This is due to the fact that the augmentation includes pilot stick position feedback ($K_{\delta_{st}}$), so the net commanded elevator deflection by the pilot becomes

$$\delta_E = K(1 - K_{\delta_{st}})\ \delta_{st}$$

where K is the actual stick gain. With his effective stick gain reduced, the pilot's contribution to commanded elevator is reduced while the augmentation's contribution is increased. The sum of the two results in the relatively constant net rms elevator with increasing augmentation. The optimum gains for the vehicle states for the three levels of augmentation is given in Table 8.

TABLE 7

AUGMENTED PERFORMANCE (rms)

	Unaugmented	Level A	Level B	Level C
Error, ε(deg)	3.05	2.50	1.12	0.31
Deflection, δ_{st}(deg)	3.71	3.64	3.51	3.68
Rate, $\dot{\delta}_{st}$(deg/sec)	7.33	6.64	5.36	5.10

σ_{a_T} = 5 g's, D = 1000 ft.

TABLE 8

OPTIMUM GAINS - TYPICAL SIGHT

	K_n	K_{aT}	$K_{\gamma T}$	K_β	K_λ	K_α	K_θ	K_q	$K_{\delta E}$	$K_{\delta s}$
1000 ft										
F^{-1} =.001	$-.138\times10^{-5}$	$-.952\times10^{-5}$	.027	.037	.014	.042	-.065	-.018	.029	.044
F^{-1} =.01	$-.819\times10^{-5}$	$-.590\times10^{-4}$	.176	.246	.102	.245	-.442	-.122	.185	.211
F^{-1} =.1	$-.298\times10^{-4}$	$-.236\times10^{-3}$	.731	1.07	.493	.872	-1.80	-.535	.689	.467

SECTION III

MULTI-AXIS ANALYSIS AND AUGMENTATION

The more challenging (and more realistic) problem of pilot-vehicle analysis and augmentation for a multi-axis air-to-air tracking task will now be considered. The dynamics of the system, as in the pitch tracking analysis in the previous section, include both vehicle and display dynamics. However, the flight condition to be considered is a highly banked turn with a normal load factor of four (i.e., 4 g turn). This involves several issues not frequently, and in some cases never, considered in previous investigations of pilot-vehicle dynamics. These extenuating issues result from the significant amount of unsymmetrical coupling between the elevation and azimuth axes of the system and the multiple control inputs involved (i.e., elevator, aileron, and rudder).

Previous investigations of multi-axis tasks have been few in number,[7] and those that have considered the effects of multi-axis aircraft control[8-10] have actually treated the dynamics of both axes independently, reducing the man's attentional allocation to each axis due to the simultaneous control task. When applicable, this approach is nice since the dynamic model is smaller and more manageable. And in wings-level flight in a position tracking task the dynamics are uncoupled, hence independent. However, in a highly-banked turn, and especially in an angular tracking or pointing task, the axes are highly interactive.

The problems to be addressed specifically in this section then include 1) the determination of any necessary changes in the pilot model parameters for multi-axis modeling from those determined from the pitch tracking analysis of Harvey,[3] and 2) the application of the pilot-optimal control

synthesis procedure to this multi-axis analysis and prediction of the improvement in performance, if any.

To accomplish the first objective, the comparison will be made between analytical, or model, results and simulation data. The data was obtained previously in the large-amplitude, motion simulator of the Flight Dynamics Laboratory, Wright-Patterson Air Force Base as part of another study performed by the Flight Dynamics Laboratory. The simulation involved F106 aircraft dynamics, and investigated several sets of display, or sight dynamics. The display to be considered here is the ideal display (or perfect director sight) considered in the previous section. The development of linearized mathematical models for the vehicle and display in this multi-axis configuration is presented in Appendices B and D of this report.

The approach to the multi-axis pilot modeling task was to attempt to match analytical and simulated statistical results in the form of rms values of system states, outputs, and control inputs. The initial objective function was a direct extension of the cost function determined experimentally by Harvey - that used in the previous section. The observation errors, neuromotor dynamics and number of control inputs were then varied to obtain the best match (via eyeball fit) of rms values. As will be seen, some additional parameters needed variation and describing functions were required in some cases.

Significant to this discussion of pilot modeling is the fact that the simulated task involved tracking a non-maneuvering target. The pilot rolled into the turn,attempted to capture the target in his display, and then tracked in approximately a steady-state condition. In terms of a linear model, this corresponds to a system with no process driving noise. In fact, the only contribution to tracking error in this case is the pilots observation and neuromotor noise. To attempt to model this situation, additive motor

noise of specified variance was injected into the pilot's control input, and the variance of this noise was chosen so as to match model and simulated rms control activity. The observation noise statistics were treated in the usual manner, that is, the variance of observation noise was specified in terms of a noise-to-signal ratio (e.g. -20 dB for full attentional allocation to a particular output quantity).

SYSTEM MODEL

For this "frozen-point" analysis, the system dynamics are linearized about a four-g, turning flight condition, the mathematical definition of which is given below.

TABLE 9

STEADY STATE PARAMETERS

Altitude, h = 10,000 ft; Mach = 0.72
Flight Velocity, U_{ss} = 775 ft/sec
Flight path angle, θ_{ss} = 0.
Bank angle, Φ_{ss} = 75.5 deg
Normal acceleration, A_z = -4g = - 128.8 ft/sec^2
Turn rate, $\dot{\psi}_{ss}$ = 0.161 rad/sec
Pitch rate, Q_{ss} = 0.156 rad/sec
Yaw rate, R_{ss} = 0.040 rad/sec
Angle of attack, α_{ss} = 14.5 deg
Elevator deflection, $\delta_{E_{ss}}$ = -20.2 deg

Furthermore, unlike a level flight condition, the engagement geometry requires a non-zero steady-state line of sight to the target, sight displayed lead angle, and relative heading between attacker and target. Since the steady-state line of sight must be a constant for this (statistically stationary) modeling approach, the engagement geometry is essentially specified once the tracking range is selected. The resulting steady-state values may then be compared to the average values obtained from simulation to verify that the simulation actually reflected a steady-state tracking condition. Finally, note that the steady-state tracking error must be zero for the perturbation quantities obtained from the linear mathematical model to be representative of total tracking error.

From the lines-of-sight equations developed in Appendix A and the display lead angle equation in Appendix B, the engagement geometry may be specified as in Table 10 for both aircraft on a common circular trajectory.

The steady-state lead angle may be found from the relations presented in Appendix B. Assuming a projectile muzzle velocity of 3300 ft/sec, a time of flight of 0.786 sec., and a ballistic jump correction, Jv, of 0.185, yields the following lead angles in the steady-state flight condition.

$$\lambda_{El_{ss}} = 0.13 \text{ rad}$$

$$\lambda_{AZ_{ss}} = -0.03 \text{ rad}$$

These lead angles are as shown in Figure 9 along with the definition of the components of the line of sight to the target. Finally, the steady-state tracking error is taken to be

$$\epsilon_{El_{ss}} = \beta_{EL_{ss}} - \lambda_{El_{ss}} = 0$$

$$\epsilon_{AZ_{ss}} = \beta_{AZ_{ss}} - \lambda_{AZ_{ss}} = 0$$

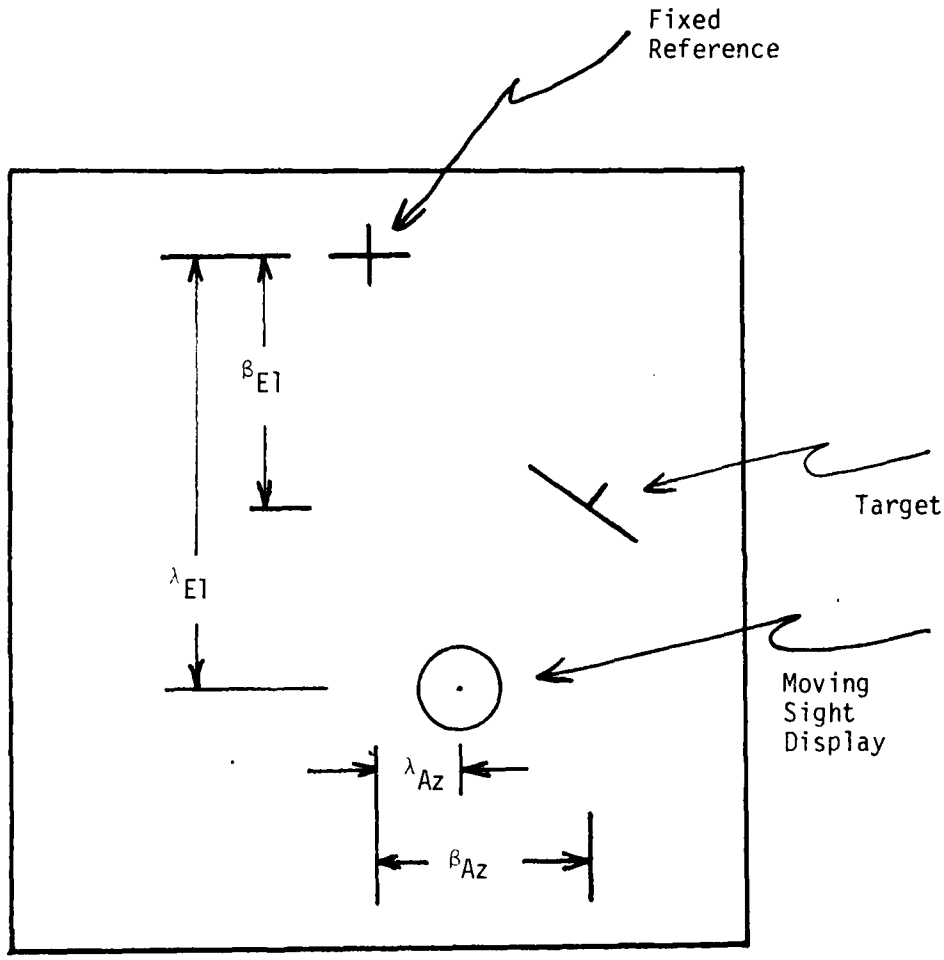

Fig. 9 Display Schematic

TABLE 10

ENGAGEMENT PARAMETERS

Target altitude, h_T = 10,000 ft; Mach = 0.72

Target Velocity, U_{SS_T} = 775 ft/sec

Target flight path angle, Θ_T = 0

Target bank angle, Φ_T = 75.5 deg

Distance to target, d = 2000 ft

Target/Attacker relative heading, $\Delta\Psi$ = 23.6°

Target normal acceleration, A_{Z_T} = -128.8 ft/sec^2

Target acceleration in attackers coordinates:

A_{T_X} = -50. ft/sec^2

A_{T_Y} = -3. ft/sec^2

A_{T_Z} = -119. ft/sec^2

Target velocity vector in attacker's coordinates:

V_{T_X} = 710 ft/sec

V_{T_Y} = 78 ft/sec

V_{T_Z} = -300 ft/sec

The comparison of the above "theoretical" steady-state with the mean value of the parameters obtained from the two simulation runs are presented in Table 11. (These two runs were the only cases for the modeled flight condition, display dynamics, etc.) It is apparent that Run 109 did not simulate the modeled steady-state situation, and checking the actual time

TABLE 11

STEADY-STATE PARAMETER

COMPARISON

	Tracking Errors (rad)		Lead Angles (rad)	
	$\varepsilon_{EL_{ss}}$	$\varepsilon_{AZ_{ss}}$	$\lambda_{El_{ss}}$	$\lambda_{AZ_{ss}}$
Theoretical	0.0	0.0	.127	-.031
Run 133	.014	.026	.123	-.045
Run 109	.003	.021	.025	-.028
	Target Velocity Components (gun coord.)		Attacker Acceleration (ft/sec^2) (body axis)		
	$V_{T_{ss}}$	$W_{T_{ss}}$ ft/sec	Ax	Ay	Az
Theoretical	78.	-300.	32.	0.	-125.
Run 133	101.	-312.	12.	-1.	-104.
Run 109	27.	- 65.	8.	-3.	- 42.
	Body Euler Angles (deg.)		Body Angular Rates (deg/sec)		
	Θ_{ss}	Φ_{ss}	P_{ss}	Q_{ss}	R_{ss}
Theoretical	3.6	75.5	- 0.6	8.9	2.2
Run 133	3.6	72.6	- 0.6	8.3	2.5
Run 109	3.4	28.9	38.0	2.9	2.6
	Velocity Angles (deg.)		Control Deflections (in.)		
	α_{ss}	β_{ss}	$\delta_{E_{st}}$	$\delta_{A_{st}}$	$\delta_{R_{ped}}$
Theoretical	14.5	0.0	-1.	0.	0.
Run 133	10.9	0.6	-2.3	-0.4	0.2
Run 109	3.8	0.6	-1.0	-0.1	1.3

histories of the parameters verified that a steady-state situation was in fact not simulated. That is, rather than constant mean values, the means were time varying for all parameters and a statistically stationary model is therefore invalid.

On the other hand, the data from Run 133 appears to agree quite well. The only discrepancy is the difference in range to the target (not given in the table). The assumed encounter geometry considered a constant range of 2000 feet, while the simulated range varied monotonically from 1800 to 3000 ft, with a mean value of 2315 feet. The primary effect of this variation is on the standard deviation of the displayed lead angle about the mean, the standard deviation is much larger than would be the case with constant range. With this in mind, however, Run 133 will be taken as the simulation results to be compared with the analytical statistics.

The linear dynamic model may now be defined, and expressed in the familiar form

$$\dot{\bar{x}} = A\bar{x} + B\bar{u}_p$$

with the state vector of perturbation variables taken as

$$\bar{x}^T = [\Delta\psi,\ v_T,\ w_T,\ d,\ \beta_{El},\ \beta_{AZ},\ \theta,\ \phi,\ \alpha,\ q,\ \beta,\ p,\ r]$$

where

$\Delta\psi$ = relative heading angle ($\psi_T - \psi_A$)

v_T, w_T = target velocity in attacker's coordinates

d = range variation

β_{El}, β_{AZ} = line of sight angle components

θ, ϕ = attacker Euler angles

α, β = angles of attack and sideslip

p, q, r = stability axis angular rates.

The pilot's control vector is

$$\bar{u}_P^T = [\delta_{E_{st}}, \delta_{A_{st}}, \delta_{R_{ped}}]$$

where as with the states, the stick and pedal deflections are perturbations from their steady state values.

The pilot's observation vector was ultimately taken to be

$$\bar{y}_p(t + \tau) = C\bar{x}(t) + D\bar{u}_p(t)$$

with

$$\bar{y}_P^T = [\varepsilon_{El}, \dot{\varepsilon}_{El}, \varepsilon_{AZ}, \dot{\varepsilon}_{AZ}, \lambda_{El}, \dot{\lambda}_{El}, \lambda_{AZ}, \dot{\lambda}_{AZ}, Ay, \phi,]$$

where

ε_{El}, ε_{AZ} = elevation and azimuth tracking error

λ_{El}, λ_{AZ} = elevation and azimuth displayed lead angle

Ay = lateral acceleration at the cockpit

ϕ = bank angle (or relative bank angle)

Note that the errors and lead angles are included as in the pitch tracking analysis of the previous section. Lateral acceleration and bank angle must now also be included in the multi-axis task with motion. These latter variables didn't need consideration in the previous analysis as it was based on a fixed-base pitch tracking experiment. They definitely must be included, however, in this more complex task with motion simulation as we shall see later.

With the steady-state parameters developed previously, and the perturbation equations developed in Appendices A, B, C, and D, the matrices A, B, C, and D in the above equation are as given in Appendix E.

To be addressed now is the coupling between the longitudinal and lateral directional axes, and the piloting "strategy" in this multi-axis task. Shown in Figure 9 previously was the schematic of the pilot's view through the heads-up display. Now one classical approach is to null the azimuth error by rolling the aircraft (using aileron and rudder) such that all the error is in the pitch axis.

This situation is depicted in Figure 10 , where for simplicity of explanation, the sight (pipper and retical) is assumed fixed in space and the pilot has rolled about the line in space represented by the sight position. It is apparent here that by using lateral-directional control, the elevation, or pitch error has been increased. Conversely, a purely pitching maneuver introduces no change in azimuth error (assuming the sight to be fixed).

This anti-symmetric cross-coupling is depicted graphically in Figure 11 , which shows the frequency response of the system's anti-symmetric transfer functions. The coupling between aileron input and elevation error is 20 to 40 dB larger than that between elevator input and azimuth error. Here, of course, the complete dynamics of the vehicle and display are included, while in the previous discussion of the display schematics we assumed the sight fixed in the display. System eigenvalues and frequency responses of the remaining transfer functions will be discussed later with augmentation results.

PILOT-VEHICLE ANALYSIS

The *baseline* pilot model was a direct extension of the pitch tracking analysis presented previously, and this model is summarized in Table 12. Reiterating the approach outlined previously, the cost function weightings in both axes are idential to those for the pitch-tracking case. The

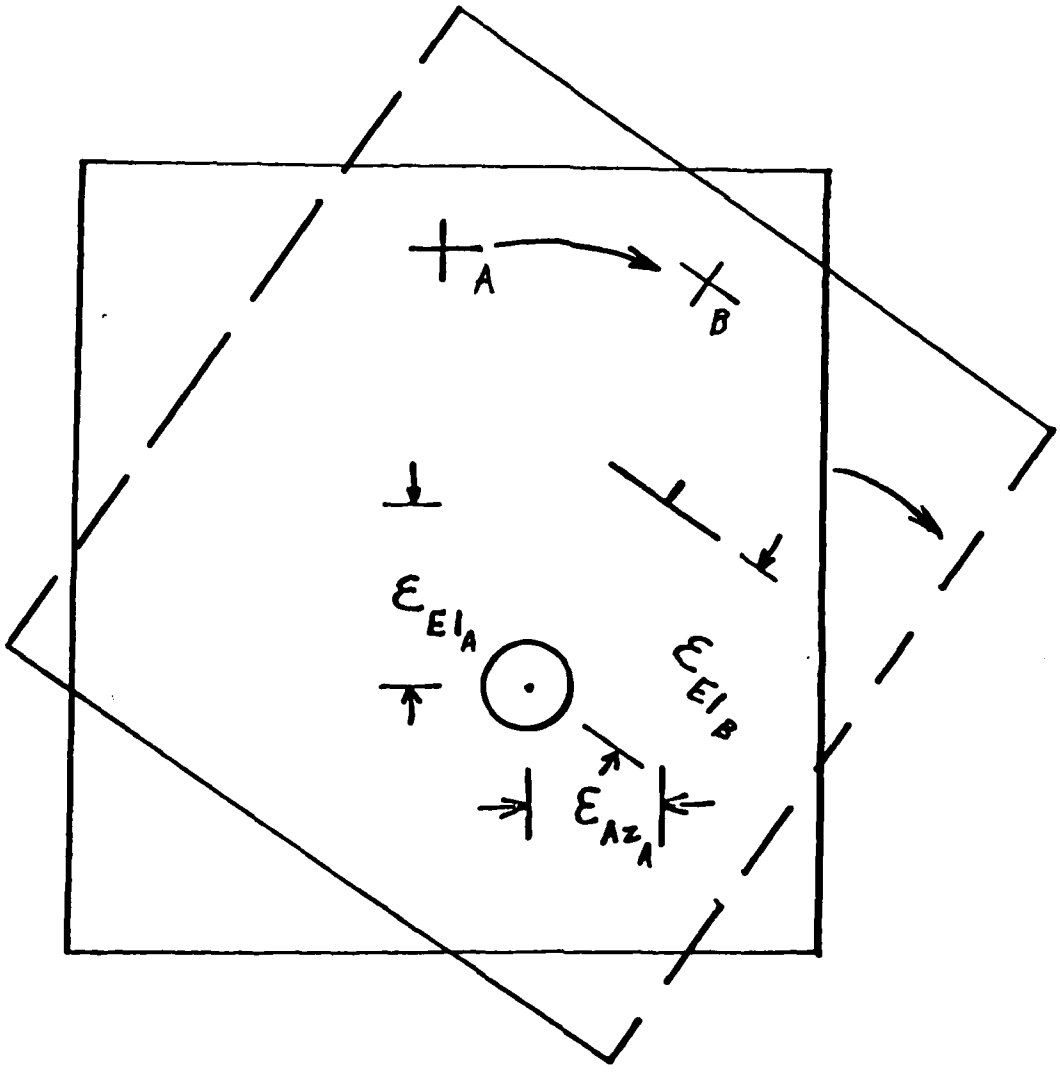

Fig. 10 Effect of Rolling on Geometry

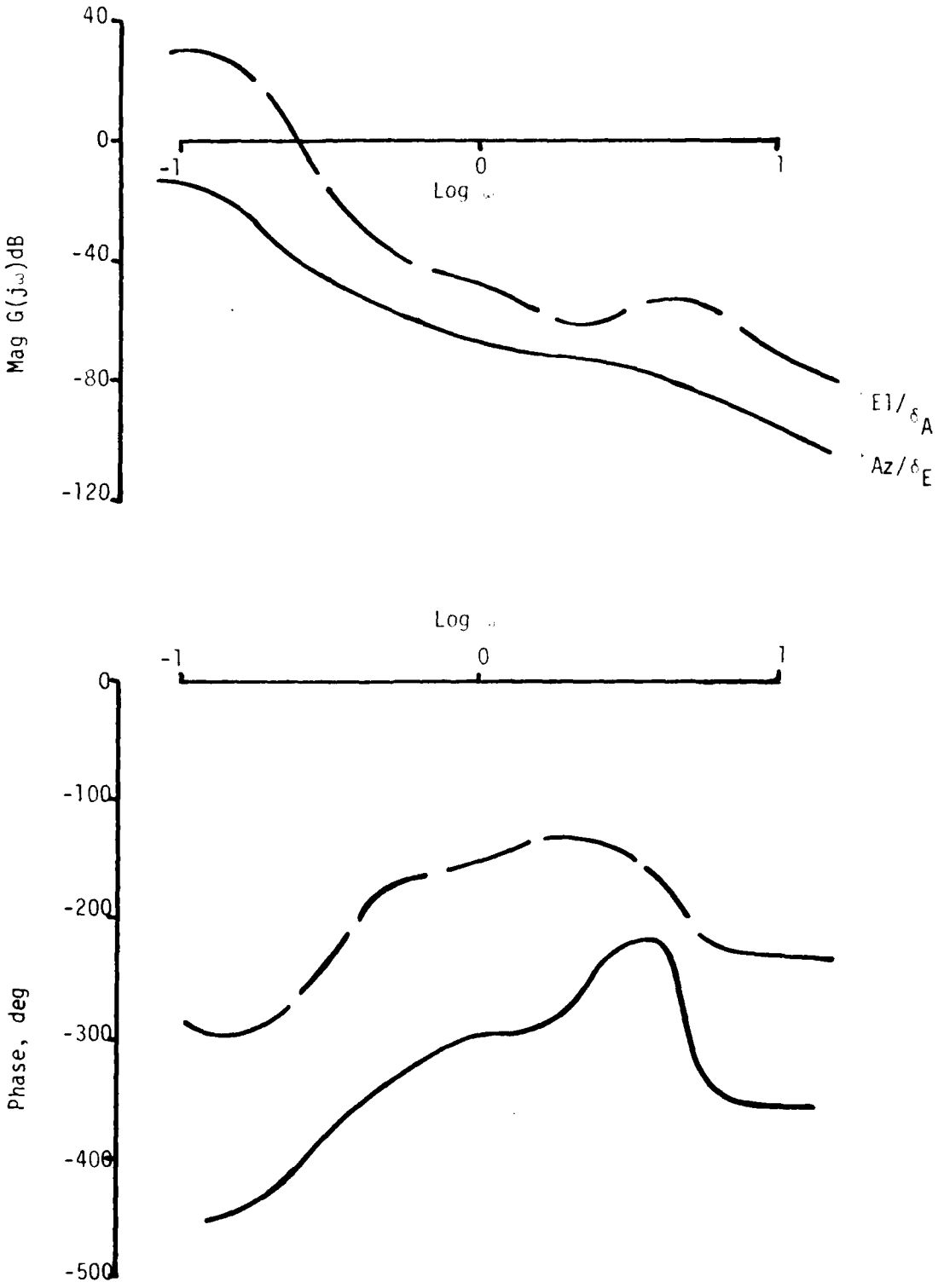

Fig. 11 Frequency Response Indicating Coupling

Table 12

BASELINE PILOT MODEL

Observation Vector, $\bar{y}^T = [\varepsilon_{El}, \dot{\varepsilon}_{El}, \varepsilon_{Az}, \dot{\varepsilon}_{Az}, \lambda_{El}, \dot{\lambda}_{El}, \lambda_{Az}, \dot{\lambda}_{Az}]$
Objective Function Weights, $Q_{\varepsilon} = 16.$, $Q_{\dot{\varepsilon}} = 1.$, $Q_{\dot{\lambda}} = 4.$ (both axes)
Observation Thresholds, $T_{\varepsilon} = T_{\lambda} = 0.05$ deg, $T_{\dot{\varepsilon}} = T_{\dot{\lambda}} = 0.10$ deg/sec
Observation Noise Ratio, = -20 dB for full attention
Fractional Attention, $f_i = 0.5$ all observed variables
Observation delay, $\tau = 0.2$ sec
Neuromuscular lag, $\tau_N = 0.2$ sec all inputs
Motor Noise Variance, varied to match rms control inputs
Control inputs, $\delta_{E_{stick}}$, $\delta_{A_{stick}}$ only

motor noise variance was modified to match model and simulated rms control activity, and the parameters determining observation noise (i.e. observation thresholds and attentional allocation) along with neuromuscular lag were varied in the attempt to match the statistics of the system states and outputs.

Initially, only two control inputs were considered, elevator and aileron stick deflection, as the importance of the rudder in this task was not clear a priori. Part of the modeling effort then was to determine the necessity for including the rudder, and it will be shown that inclusion is warranted.

Finally, recall that the target is not maneuvering, so the magnitude

of the motor noise variances must be specified rather than noise-to-signal ratio, the more typical case. The resulting noise-to-signal ratio obtained from matching control activity is then one of the modeling results in this analysis.

The comparison of the baseline model results with those obtained from simulation is shown in Table 13. Considering the use of essentially a "single axis" model, the results are amazingly good, the largest differences appearing in lead angles, bank (ϕ) and side-slip angle (β), and higher angular rates resulting from the model.

To assess the first-order sensitivities of the rms performance to increased observation errors and pilot bandwidth (i.e. neuromuscular lag), two "perturbations" to the baseline model were evaluated. The first involved reducing the fractional attention allocation from 0.5, the inverse of the number of controlled axes, to 0.125, the inverse of the dimension of the observation vector. Additionally, the threshold on angular rate was increased from 0.1 to 0.18 deg/sec consistent with some earlier studies.[11] The second case considered the above changes plus increased the neuromuscular lag time constant from 0.2 seconds to 0.3 seconds for both control inputs.

The results for these two additional models are shown in Table 14, along with the baseline model results. The effect of the increase in the observation noise due to reduced attentional capacity and increased threshold is an increase in all rms values of states and outputs. But this is as expected since increased observation noise is similar to increased motor noise in effect. Note, however, that the increases appear to be greater in the lateral axis, with rms azimuth error (ϵ_{Az}) increasing 65 percent and side-slip angle (β) and roll rate (p) increase 10 percent.

It would appear that the lateral-directional axis, then, is more sensitive to observation errors, may require increased attentional allocation, and tends to contribute most to the task difficulty.

The effect of increased neuromuscular lag on both control inputs also appears to affect the lateral axis more than the longitudinal - the azimuth error increasing significantly more than the longitudinal. As would be expected, all three angular rates decreased, but these were higher than the simulated values for all three models - thus indicating perhaps that neuromuscular lag greater than 0.2 seconds is warranted.

TABLE 13

SIMULATION VS. BASELINE MODEL

RMS PERFORMANCE

	Tracking Error (deg)		Lead Angles (deg)	
	ε_{El}	ε_{Az}	λ_{El}	λ_{Az}
Simulated	1.09	0.97	1.72	2.58
Model	1.31	0.82	0.74	0.34
	Target Velocities (ft/sec)		Euler Angles (deg)	
	w_T	v_T	θ	ϕ
Simulated	48.	34.	1.09	4.18
Model	37.	15.	0.74	2.29
	Velocity Angles (deg)		Angular Rates (deg/sec)	
	α	β	p	q r
Simulated	1.40	0.20	4.99	1.72 0.92
Model	1.03	0.43	6.07	3.04 1.72
	Control Inputs (in)			
	$\delta_{E_{ST}}$	$\delta_{A_{ST}}$	$\delta_{R_{PED}}$	
Simulated	0.27	0.22	0.22	
Model	0.28	0.23	—	

TABLE 14

THREE BASIC MODELS-RMS PERFORMANCE

	Tracking Error (deg)		Lead Angles (deg)	
	ε_{El}	ε_{Az}	λ_{El}	λ_{Az}
Baseline	1.43	0.80	0.74	0.34
Incr. Obs. Err.	1.60	1.32	0.97	0.52
Obs. Err. & Lag	1.66	1.95	0.34	0.69
	Target Velocities (ft/sec)		Euler Angles (deg)	
	w_T	v_T	θ	ϕ
Baseline	37.	15.	0.74	2.29
Incr. Obs. Err.	44.	22.	0.97	3.32
Obs. Err. & Lag	21.	29.	1.38	4.70
	Velocity Angles (deg)		Angular Rates (deg/sec)	
	α	β	p	q r
Baseline	1.03	0.43	6.07	3.04 1.72
Incr. Obs. Err.	1.09	0.47	6.65	3.09 1.78
Obs. Err. & Lag	1.15	0.40	6.30	2.58 1.38
	Control Inputs (in)		Motor Noise Ratio (dB)	
	$\delta_{E_{ST}}$	$\delta_{A_{ST}}$	$\delta_{E_{ST}}$	$\delta_{A_{ST}}$
Baseline	0.28	0.23	-10	-12.3
Incr. Obs. Err.	0.28	0.27	-10	-13.6
Obs. Err. & Lag	0.24	0.25	- 8	-11.1

Furthermore, though neuromuscular lag time constants on the order of 0.1 seconds for a single-axis task and a force-sensitive, side-arm control stick may be reasonable, higher time constants are appropriate for a movable center-stick control, and even larger time constants, approaching one second, for rudder pedals in this multi-axis task.

Finally, none of these models were able to match the much higher simulated lead angles (λ_{El} and λ_{Az}). Furthermore, none of the other models to be discussed below yielded significantly larger rms lead angles. The answer probably lies in the fact that the simulation run, although almost representative of a true steady-state aircraft flight condition, did not result in a constant range to the target. The range increased from the smallest value of 1800 feet, occurring early in the simulation, to over 3000 feet at the end of the 40 second run. Consequently, the projectile time of flight to the target increased proportionally. Since the lead angle tends to be proportional to the time of flight, the lead angles at the larger ranges later in the simulation run are significantly higher than those occurring earlier in the run, which are closer to the modeled constant range of 2000 feet. Hence the rms lead angles obtained from the simulation would be expected to be larger than those prediced via the model.

The fact that the largest deviation is in the azimuth lead angle is consistent with this reasoning as well. At the highly banked flight condition considered ($\phi \simeq 75°$), the largest component of the gravity vector will be in the azimuthal direction rather than in the elevational. Hence, the azimuth lead angle will be more effected by the "gravity drop" of the projectile, and therefore experience the largest increase as the time of flight increases.

As a result of these considerations, we shall consider the aircraft

states as the most important for comparison purposes, followed by the tracking errors, and finally the lead angles. As a final note regarding the matching of rms performance, the simulation run represents a single case involving a single pilot, hence is in effect a single data point. On the other hand, the statistical results from the model represents ensemble data over a large sample ($N \to \infty$). Therefore, too much emphasis on precise matching is foolish.

With these initial results in hand, we shall now address the issue of the inclusion of the third control input, the rudder pedal.

Adding the third control parameter to the model, utilizing a pre-selected neuromuscular time constant, must be done with care. The two lateral-directional controls (aileron and rudder) do not yield pure modal responses. That is, an aileron deflection produces both roll and yaw, as is the case with the rudder as well. Recalling the control equation for the pilot model as

$$T_N \dot{\bar{u}}_p = -K_1 \hat{\bar{x}} - \bar{u}$$

the result of this coupled response is a nondiagonal T_N matrix. Therefore, the eigenvalues of T_N represent the effective neuromuscular lag as before, but this lag is for a combination of control inputs described by the eigenvectors of T_N. Therefore, the eigenvalues of T_N will be used for the lag time constants, realizing that rather than representing a <u>pure</u> aileron input, for example, the appropriate time constant (or eigenvalue) represents <u>primarily</u> aileron input along with some lesser rudder input.

The model results with rudder included are given in Table 15, along with the simulated results. Note that the three-control model includes the higher observation noises (fractional attention of 0.125 and angular rate thresholds of 0.18 deg/sec) as well as the larger elevator

TABLE 15

BASIC THREE-CONTROL MODEL PERFORMANCE

	Tracking Error (deg)		Lead Angles (deg)	
	ε_{El}	ε_{Az}	λ_{El}	λ_{Az}
Simulated	1.09	0.97	1.72	2.58
Model	1.66	1.03	0.97	0.47
	Target Velocities (ft/sec)		Euler Angles (deg)	
	w_T	v_T	θ	ϕ
Simulated	48.	34.	1.09	4.18
Model	46.	20.	0.92	2.58
	Velocity Angles (deg)		Angular Rates (deg/sec)	
	α	β	p	q r
Simulated	1.40	0.20	4.99	1.72 0.92
Model	0.97	0.63	5.44	2.52 1.32
	Control Inputs (in)		Neuromotor Lags (sec)	
	$\delta_{E_{ST}}$	$\delta_{A_{ST}}$ $\delta_{R_{PED}}$	τ_{NE}	τ_{NA} τ_{NR}
Simulated	0.27	0.22 0.22	--	-- --
Model	0.22	0.39 0.28	0.3	0.3 1.1

lag (0.3 seconds). And therefore is similar to the third model for which the results are given in Table 14.

First note that much higher lag on the rudder input was required. Attempting to use a lag time constant of around 0.3 seconds for all three controls resulted in lateral directional control inputs an order of magnitude higher than those shown. Also, one would expect a higher lag for pedal controls than for stick.

Note that most of the rms values for this three-control model are closer to the simulated results than the similar two-control model (the third set of results given in Table 14). The exceptions are in the much higher side-slip (β) and much lower bank angle (ϕ). We'll return to this later.

First consider the results depicted in Figure 12, which gives the aileron-to-azimuth-error pilot describing functions obtained from the two- and three-control models. These describing functions are equivalent to those given in the pitch-tracking analysis of the previous section in that they are comparable to those for a compensatory task. Note that the low frequency phase of the two-control-model result is zero, while that of the three control model is near -270 degrees. This fact, along with the comparison of the low frequency slopes of the magnitude plots (zero for two controls, -20dB per decade for three controls)indicates that the describing function gains are of opposite sign! Which one is correct?

We will only be able to answer part of that question here. One sign on the describing function corresponds to a piloting strategy of rolling to null azimuth error. This is the only possibility if aileron is the only control input. However, with both control inputs, the possibility of

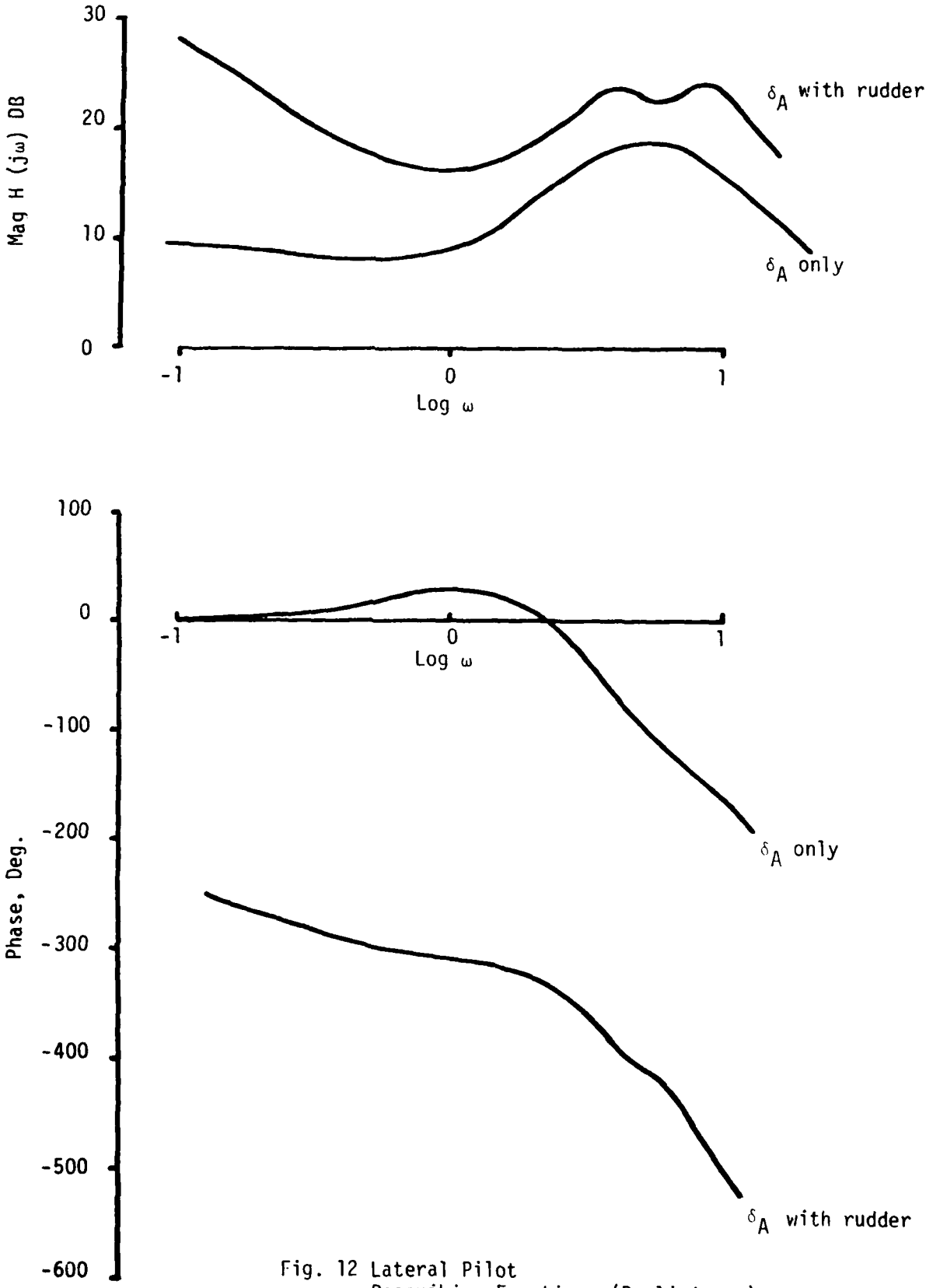

Fig. 12 Lateral Pilot
Describing Functions (Preliminary)

a pointing rather than a rolling strategy is possible, with "cross control" inputs being used. Inclusion of the rudder is necessary, then, to allow either strategy to be used, and the existence of opposite sign on the three-control aileron describing function would represent the effects of "pointing". The preliminary conclusion then, would appear that inclusion of the rudder may be necessary to capture the proper piloting strategy "Which strategy is correct?" is now the question.

Now let's reconsider the rms performance of the three-control model in Table 15, and note the much higher value for rms side-slip angle (β) and the lower rms bank angle (ϕ) compared to the previous two-control models (Table 14). The fact that the rms azimuth error is reduced in the three-control case, along with the large increase in side-slip and lower bank angle further supports the presence of a "pointing" rather than "rolling" strategy. Here the pointing may be accomplished with rudder input, however. But the fact that the simulation results show much lower side slip indicate that the rolling strategy was actually used. This leads to the conclusion that the original objective function (weighting only displayed errors and lead angles) is insufficient to correctly model the pilot's strategy in the lateral-directional axis.

To determine the required modification to the objective function, we must consider what additions to the pilot's observation vector are appropriate. (Comments from a test pilot, incidentally, were helpful in this regard.) In addition to lead angles and tracking error (or line of sight), the pilot also sees the target itself through the heads-up display. Consequently, target bank angle and heading, or more precisely, relative bank angle and heading are observed, although in this in-plane

maneuver, the relative heading was considered difficult to observe accurately. However, relative bank angle was observable, and intuitively, if nothing else, would appear to be important. Furthermore, in the purely single axis experiments of Harvey, target and attacker bank angle were both always zero, hence no importance of bank angle could be ascertained from his analysis.

This raises another key point not previously considered. Harvey's experiments were fixed base, while in the Air Force LAMARS facility, motion cues, and particularly accelerations, were most definately available. Furthermore, clear evidence is available[12] that pilots avoid lateral accelerations, while vertical accelerations of reasonable magnitude (e.g. less than 5 to 6 g's) are not as highly disliked, or at least pilots are more conditioned to the latter type. Consequently, inclusion of relative bank angle and lateral acceleration in the observation vector is clearly reasonable, and weighting both of these parameters in the objective function is consistent with this entire discussion of piloting strategy.

To complete the model then the observation threshold on relative bank angle was taken to be 5 degrees, based on the pilot's perception thresholds of 0.05 degrees at the pilot's eye, tracking range of 2000 ft., and target wing span of approximately 40 feet. The perception threshold on lateral acceleration was assumed to be 0.4 ft/second or 0.012 g's, roughly consistent with some earlier studies.[13] Finally, using an analysis similar to that above for bank angle, it was determined that the threshold on relative bank angle rate is approximately 10 deg/sec. But since this is much larger than the rms roll rates (p) encountered, no useful information could be gained by including roll rate in the observation vector.

Inclusion of the above parameters results in the multi-axis pilot model summarized in Table 16 . Note that since the target has a constant bank angle, observing and weighting relative bank angle is equivalent to observing and weighting the attacker's bank angle in this case. Finally, the attentional allocation has been adjusted to further improve the model results, and these allocations reflect the relative difficulty, or workload, between the two axes.

With the above model, the rms performance shown in Table 17 was obtained. The parameters marked with the double asterisk indicate this value was the closest to the simulated value of all models considered, while the single asterisk denotes one other model considered resulted in a closer match for that parameter. Considering all the factors discussed, it is felt that this model is quite justified.

SYSTEM AUGMENTATION

With this final pilot model established, we may proceed with the system augmentation. Reiterating the methodology, with augmentation, the system dynamics are represented as

$$\dot{\bar{x}} = A\bar{x} + B_p\bar{u}_p + B_A\bar{u}_A + \bar{w}$$

where $\bar{u}_p$ and $\bar{u}_{aug}$ are the vectors of control inputs of the pilot and augmentation, respectively, while $\bar{w}$ represents any system disturbances. The control $\bar{u}_{aug}$ is chosen, then, to minimize the objective function.

$$J_{aug} = J_p + E\left\{\lim_{T\to\infty} \frac{1}{T} \int_0^T \bar{u}'_{aug}\, F\bar{u}_{aug}\, dt\right\}$$

TABLE 16

FINAL MULTI-AXIS
PILOT MODEL

Observation Vector, $\bar{y}^T = [\varepsilon_{El}, \dot{\varepsilon}_{El}, \varepsilon_{Az}, \dot{\varepsilon}_{Az}, \lambda_{El}, \dot{\lambda}_{El}, \lambda_{Az}, \dot{\lambda}_{Az}, a_y, \phi_{rel}]$

Objective Function Weights, $Q_\varepsilon = 16.$, $Q_{\dot{\varepsilon}} = 1.$, $Q_{\dot{\lambda}} = 4.$, $Q_{a_y} = .007$, $Q_\phi = 8.$

Observation Thresholds, $T_\varepsilon = T_\lambda = .05$ deg, $T_{\dot{\varepsilon}} = T_{\dot{\lambda}} = .18$ deg/sec

$T_{a_y} = .4$ ft/sec^2, $T_\phi = 5$ deg

Fractional Attention Allocations, $f_i = .05$ on ε_{El}, $\dot{\varepsilon}_{El}$, λ_{El}, $\dot{\lambda}_{El}$

$f_i = .15$ on ε_{Az}, $\dot{\varepsilon}_{Az}$, λ_{Az}, $\dot{\lambda}_{Az}$

$f_i = .1$ on a_y and ϕ

Observation Noise Ratio -20dB for full attention

Observation Delay, $\tau = 0.2$ sec

Neuromuscular Lag, $\tau_N = .33$ on $\delta_{E_{st}}$ (obj. func. wt. = .05)

$\tau_N = .23$ on $\delta_{A_{st}}$ (obj. func. wt. = .10)

$\tau_N = .62$ on $\delta_{R_{ped}}$ (obj. func. wt. = .12)

Motor Noise Ratios, $V_n = \pi\rho_u\sigma_u^2$

$\rho_u = .05$ (-8 dB) on $\delta_{E_{st}}$

$\rho_u = .02$ (-12 dB) on $\delta_{A_{st}}$

$\rho_u = .05$ (-8 dB) on $\delta_{R_{ped}}$

TABLE 17

FINAL MODEL PERFORMANCE

	Tracking Error (deg)		Lead Angles (deg)	
	ϵ_{El}	ϵ_{Az}	λ_{El}	λ_{Az}
Simulated	1.09	0.97	1.72	2.58
Final Model	1.78	1.72	1.38**	0.63*
	Target Velocities (ft/sec)		Euler Angles (deg)	
	w_T	v_T	θ	ϕ
Simulated	48.	34.	1.09	4.18
Final Model	63.	25.*	0.97*	3.55*
	Velocity Angles (deg)		Angular Rates (deg/sec)	
	α	β	p	q r
Simulated	1.40	0.20	4.99	1.72 0.92
Final Model	0.97	0.15**	5.21**	2.58** 0.57**
	Control Inputs (in)		Neuromotor Lags (sec)	
	$\delta_{E_{st}}$	$\delta_{A_{st}}$ $\delta_{R_{ped}}$	τ_{NE}	τ_{NA} τ_{NR}
Simulated	0.27	0.22 0.22	--	-- --
Final Model	0.23	0.15 0.10	.33	.28 .62
	Lateral Acceleration (ft/sec^2)		Neuromotor Noise Ratios (dB)	
	a_y		N_{δ_E}	N_{δ_A} N_{δ_R}
Simulated	0.67		--	-- --
Final Model	0.78**		-8	-12 -8

where J_p is the pilot's objective function as determined previously in the pilot/vehicle analysis. The optimal control law is then (as shown previously)

$$\bar{u}_{aug} = -F^{-1}(B_A^T K_{A_1} \bar{x} + B_A^T K_{A_2} u_p)$$

where K_{A_1} and K_{A_2} are determined by solving the pilot and augmentation Riccati equations simultaneously. The augmented piloted system may then be represented

$$\dot{\bar{x}} = (A - B_A F^{-1} B_A^T K_{A_1})\bar{x} + (B_p - B_A F^{-1} B_A^T K_{A_2})\bar{u}_p + \bar{w}$$

or $(A - B_A F^{-1} B_A^T K_{A_1}) = (A - B_A K_x)$ = augmented plant matrix

$(B_p - B_A F^{-1} B_A^T K_{A_2}) = (B_p - B_A K_u)$ = augmented control matrix

(e.g., stick gains and cross feeds)

The pilot's control law remains

$$\dot{\bar{u}}_p = -G^{-1} B_p^T K_{P_1} \dot{\bar{x}} - G^{-1} B_p^T K_{P_2} \bar{u}_p$$

except the Riccati gains K_{P_1} and K_{P_2} now reflect the presence of augmentation as they are solved simultaneously with the augmentation problem using the augmented plant matrices.

The open- and closed-loop root loci as augmentation level increases from unaugmented (denoted by U) to higher levels of augmentation (denoted 1-4) are shown in Figures 13 and 14 . The first figure shows the (primarily) longitudinal eigenvalues, recognizing this system actually has coupled longitudinal and lateral-directional modes, with the second figure depicting the (primarily) lateral-directional roots. As with the pitch tracking results of the previous section, the augmented system roots are denoted as "X" and the piloted closed-loop roots are denoted as "O".

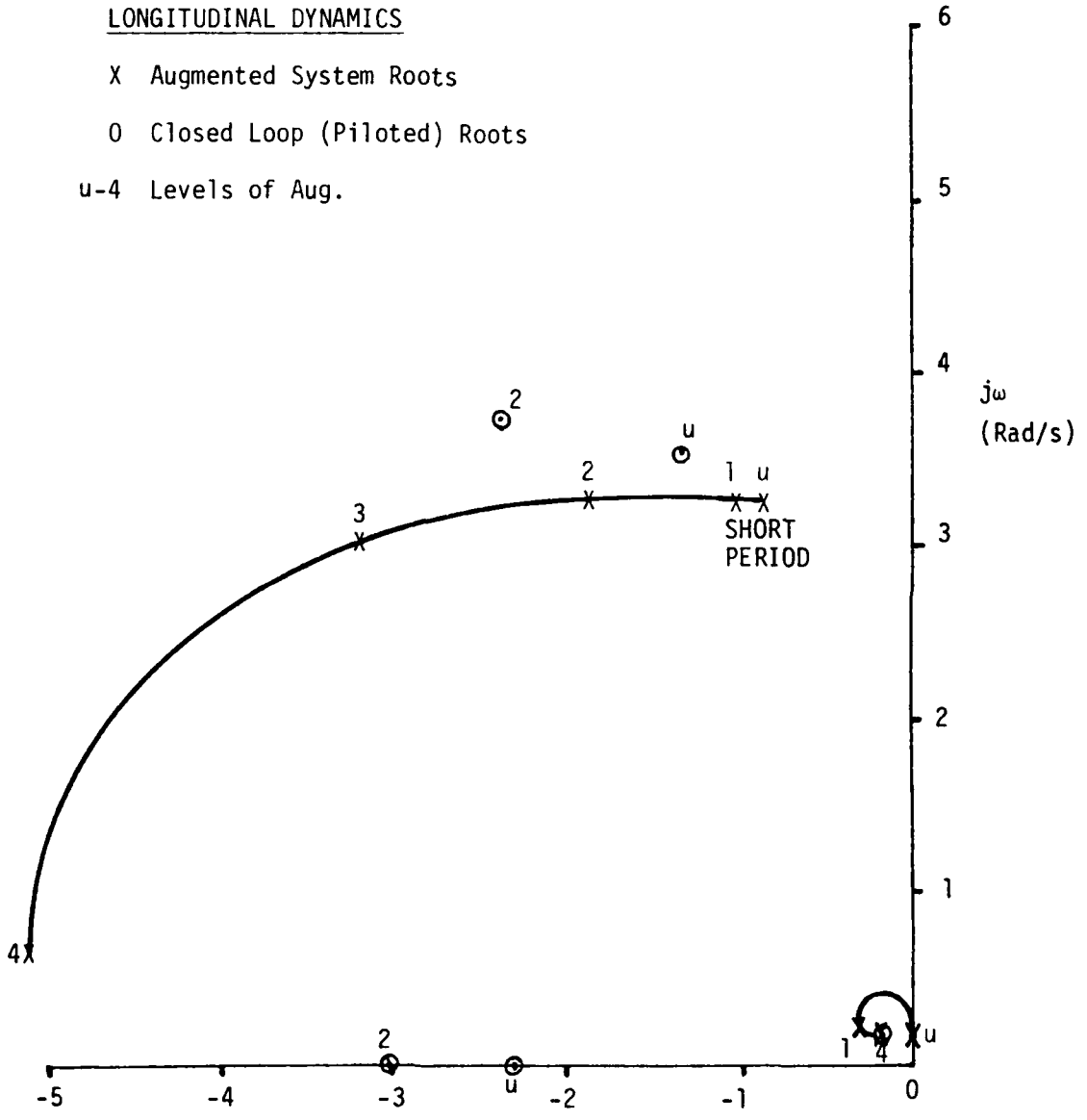

Fig. 13 Longitudinal Root Locus

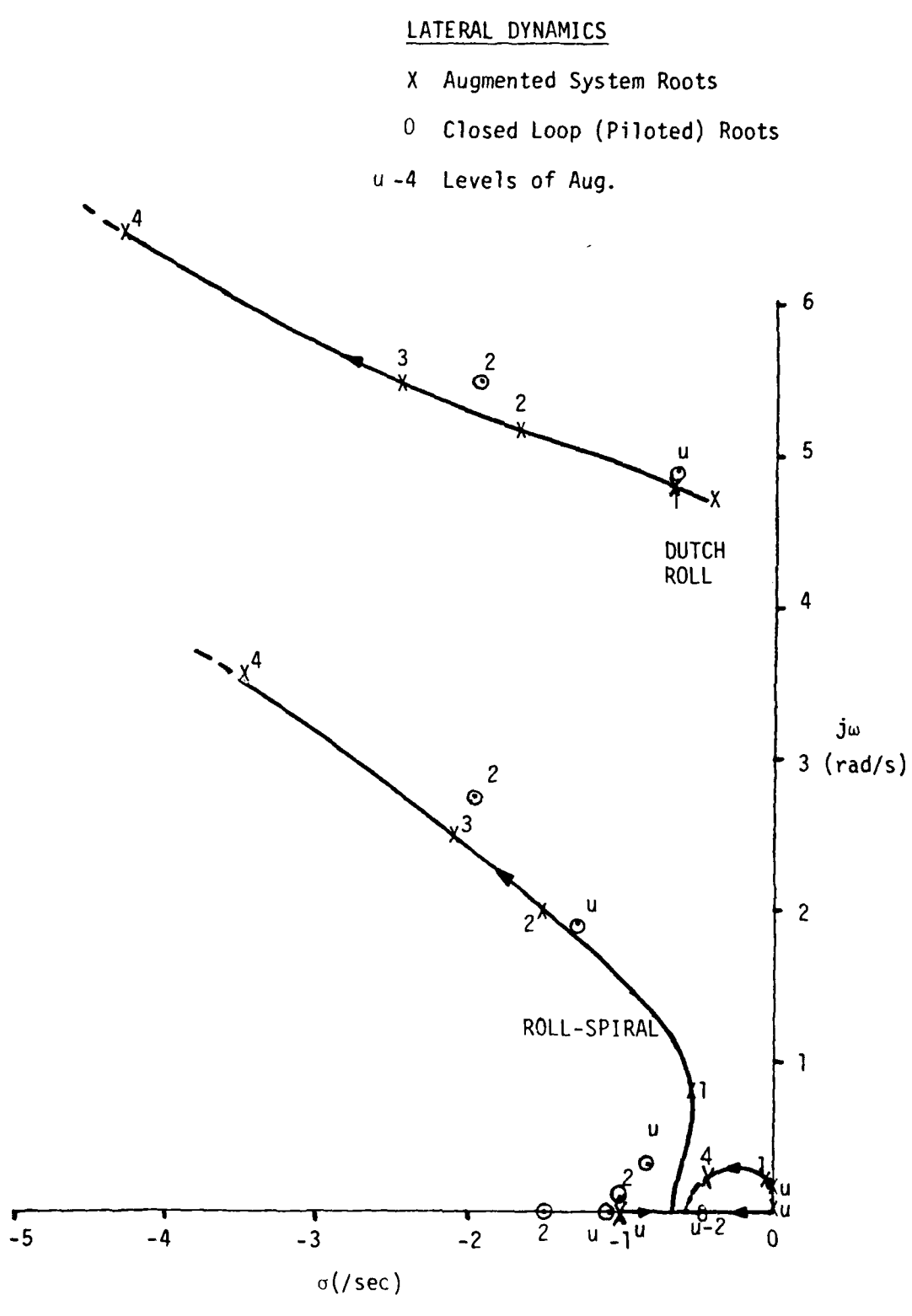

Fig. 14 Lateral Root Locus

Examination of the longitudinal root locus leads to the conclusion that the trends are changed only slightly from those obtained in the single-axis pitch-tracking analysis. The two low frequency roots from the geometry and kinematics of the problem were at the origin for the wings-level pitch analysis, but still move quickly toward the invariant, low-frequency pair of piloted closed-loop roots with augmentation. Recall this probably indicates the existance of a pair of pseudo-zeros or transmission zeros at this point. The trend in the vehicle short-period roots is also similar to previous results, with the exception that short period damping is increased much more due to augmentation. Finally, the proximity of the open-loop roots to the closed-loop roots for the unaugmented plant (U) and level-two augmented plant (2) indicate less compensation being introduced by the pilot, primarily due to his reduced bandwidth (τ_n = .3 instead of τ_n = .1) in this more complex task.

The root loci for the lateral-directional axis will now be considered. The unaugmented system has two eigenvalues near $\pm$ .2j associated with the azimuth portion of the geometry and kinematics of the engagment, the spiral and roll subsidence vehicle roots at the origin and near -1 per second, respectively, and the dutch roll roots at -.4 $\pm$ 4.7j rad/sec. With augmentation now, the damping and frequency of the dutch roll are increased, and a complex roll/spiral mode is formed from the spiral and roll subsidence roots. The two low-frequency roots on the $j\omega$ axis ultimately attach to the real axis near -.6 and become two real roots. The first of these approaches the invariant closed-loop root at -.5/sec, the other moves to the left on the real axis. This latter root, incidently, appears to be attracted to the pilot closed-loop roots near -1/sec which also approach the real axis with increased augmentation. Finally, associated

with the dutch-roll and the roll-spiral are two pairs of piloted closed-loop roots very close to their associated unagumented branches.

Except for the roll-spiral mode without augmentation, the pilot appears to introduce relatively little compensation in terms of eigenvalue repositioning, again due to the complexity of this multi-variable task and his limited bandwidth. The relatively large importance of this roll/spiral mode could be inferred from this result.

The level-two augmentation was selected for evaluation and it appears to represent a medium-to high-level of augmentation. (The gains K_x and K_u are given in Table 18 for all augmentation levels). The frequency response for the system and pilot describing functions are presented in Figures 15 to 20 for unaugmented and augmented systems.

The longitudinal results shown in Figure 15 indicate the near cancellation of the low frequency eigenvalues due to closure of the tracking loop, and increased damping of the short-period mode (near 3.5 rad/sec) is evident. The pilot's describing function shown in Figure 16 shows little change due to augmentation.

The aileron frequency responses are given in Figures 17 and 18 . The phase results for the unaugmented vehicle clearly show the presence of the spiral root at the origin, as well as the two low-frequency kinematic roots. These three roots appear to be effectively cancelled with augmentation.

The pilot's aileron describing function indicates almost a constant aileron-to-error-rate tracking characteristic, or

$$y_p(s) = \frac{\delta_A(s)}{\dot{\epsilon}_{Az}(s)} = - K_p e^{-\tau s}$$

With augmentation, the slope of the magnitude curve is reduced, implying lesser emphasis on rate. This should indicate less pilot workload as measured by lead requirements.

TABLE 18

AUGMENTATION GAINS

		$K_{\dot{v}}$	K_{v_T}	K_{w_T}	K_d	$K_{\beta_{El}}$	$K_{\beta_{Az}}$	K_θ	K_ϕ	K_α	K_q	K_β	K_p	K_r
Level 1	δ_E	-0.004	-0.00005	-0.0005	-0.00003	-0.730	-0.022	0.003	-0.015	0.960	-0.402	0.030	0.004	0.005
	δ_A	-0.0009	0.002	-0.000004	-0.00004	0.028	1.03[illegible]	-0.042	-0.368	-0.013	0.008	-0.105	-0.440	-0.755
	δ_R	-0.0005	0.0008	-0.000003	-0.00002	0.014	0.546	-0.022	-0.100	-0.010	-0.0003	0.935	-0.150	-1.167
Level 2	δ_E	-0.033	-0.0004	-0.004	-0.0003	-5.811	-0.148	0.023	-0.117	5.912	-3.197	0.343	0.023	0.033
	δ_A	-0.005	0.009	-0.00004	-0.0002	0.127	5.470	-0.105	-1.977	-0.031	0.044	-9.485	-1.838	-2.206
	δ_R	-0.003	0.005	-0.00002	-0.0001	0.075	3.585	-0.081	-0.334	-0.026	-0.001	7.517	-0.479	-5.701
Level 3	δ_E	-0.060	-0.0007	-0.007	-0.0004	-10.44	-0.252	0.038	-0.209	8.950	-5.652	0.606	0.040	0.057
	δ_A	-0.008	0.014	-0.00007	-0.0004	0.193	8.881	-0.081	-3.314	-0.035	0.07[illegible]	-20.40	-2.705	-2.952
	δ_R	-0.006	0.009	-0.00005	-0.0002	0.122	6.451	-0.110	-0.536	-0.033	-0.003	17.19	-0.711	-9.242
Level 4	δ_E	-0.132	-0.001	-0.015	-0.0009	-23.18	-0.521	0.076	-0.468	14.79	-12.06	1.211	0.092	0.119
	δ_A	-0.017	0.028	-0.0001	-0.0008	0.377	18.17	0.060	-6.975	-0.046	0.177	-55.59	-4.687	-4.792
	δ_R	-0.013	0.018	-0.0001	-0.0005	0.216	14.20	-0.128	-1.073	-0.036	-0.013	52.77	-1.196	-17.04

		Level 1		Level 2		Level 3		Level 4	
		K_{δ_E}	K_{δ_A}	K_{δ_E}	K_{δ_A}	K_{δ_E}	K_{δ_A}	K_{δ_E}	K_{δ_A}
	δ_E	0.058	-0.0006	0.318	-0.002	0.443	-.003	0.610	-0.003
	δ_A	-0.0006	0.131	-0.001	0.372	-0.001	0.459	-0.001	0.576
	δ_R	-0.0006	0.052	-0.001	0.056	-0.002	0.040	-0.002	0.017

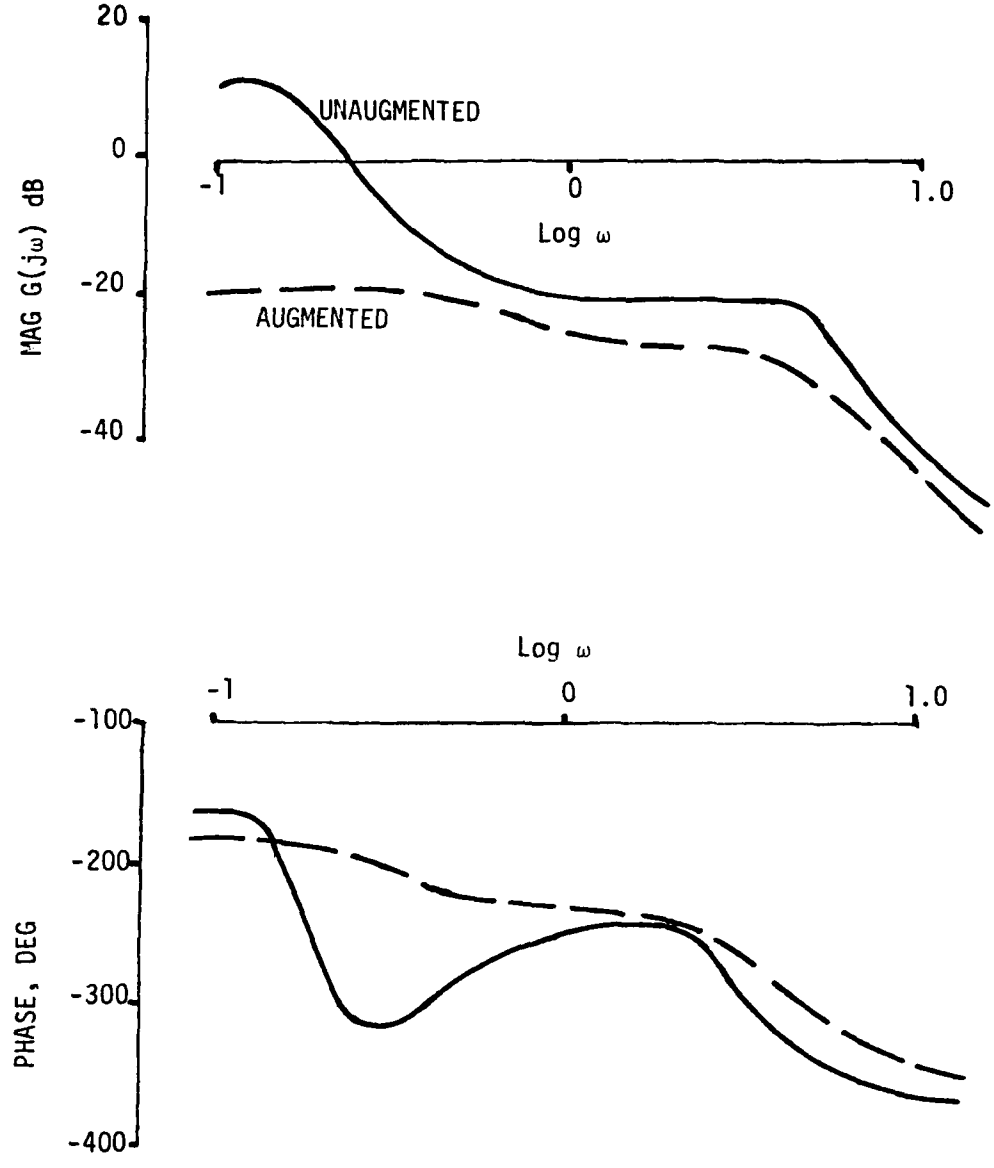

Fig. 15 Vehicle Describing Function $_{E1}/\delta_E$

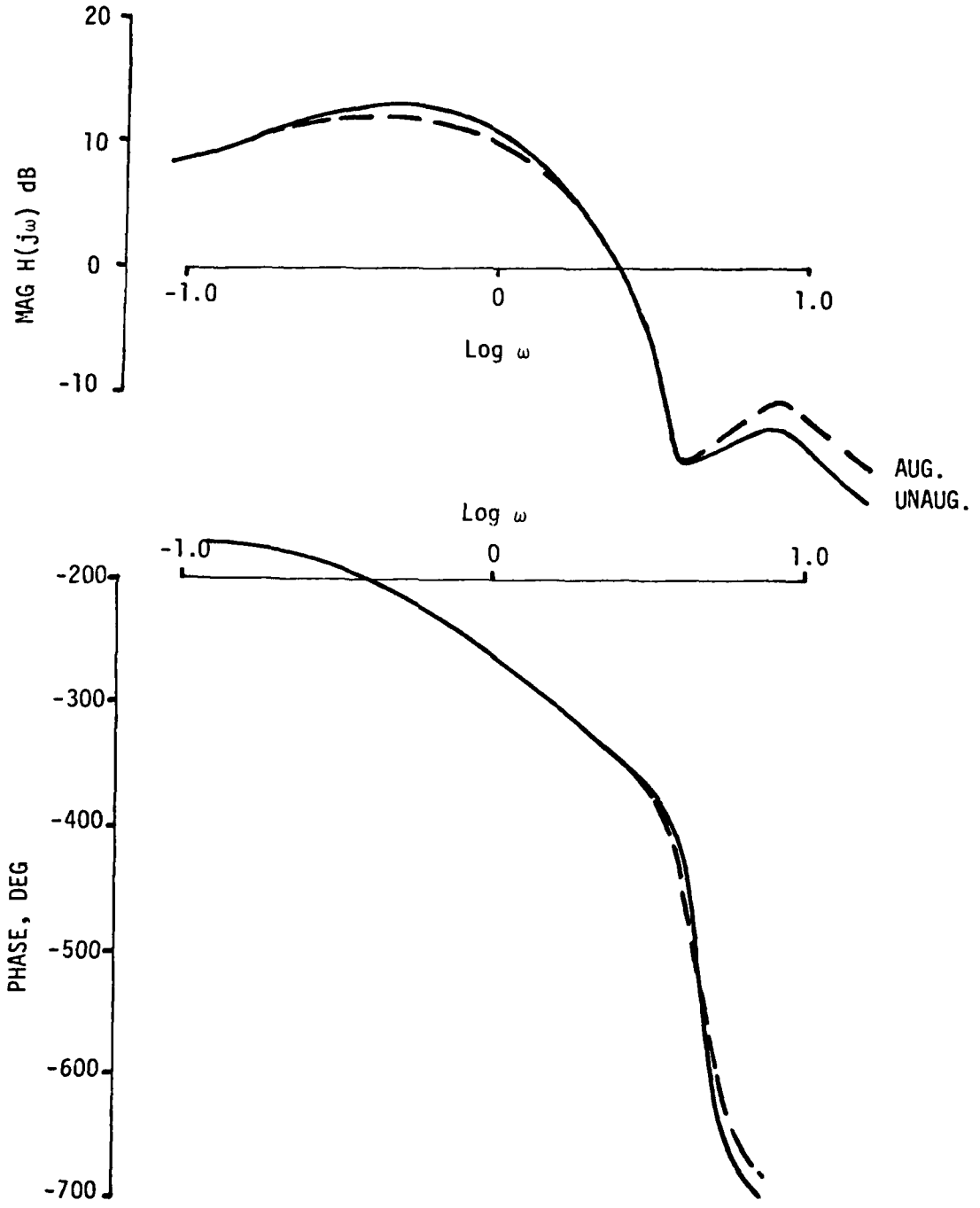

Fig. 16 Pilot's Describing Function δ_E/ϵ_{E1}

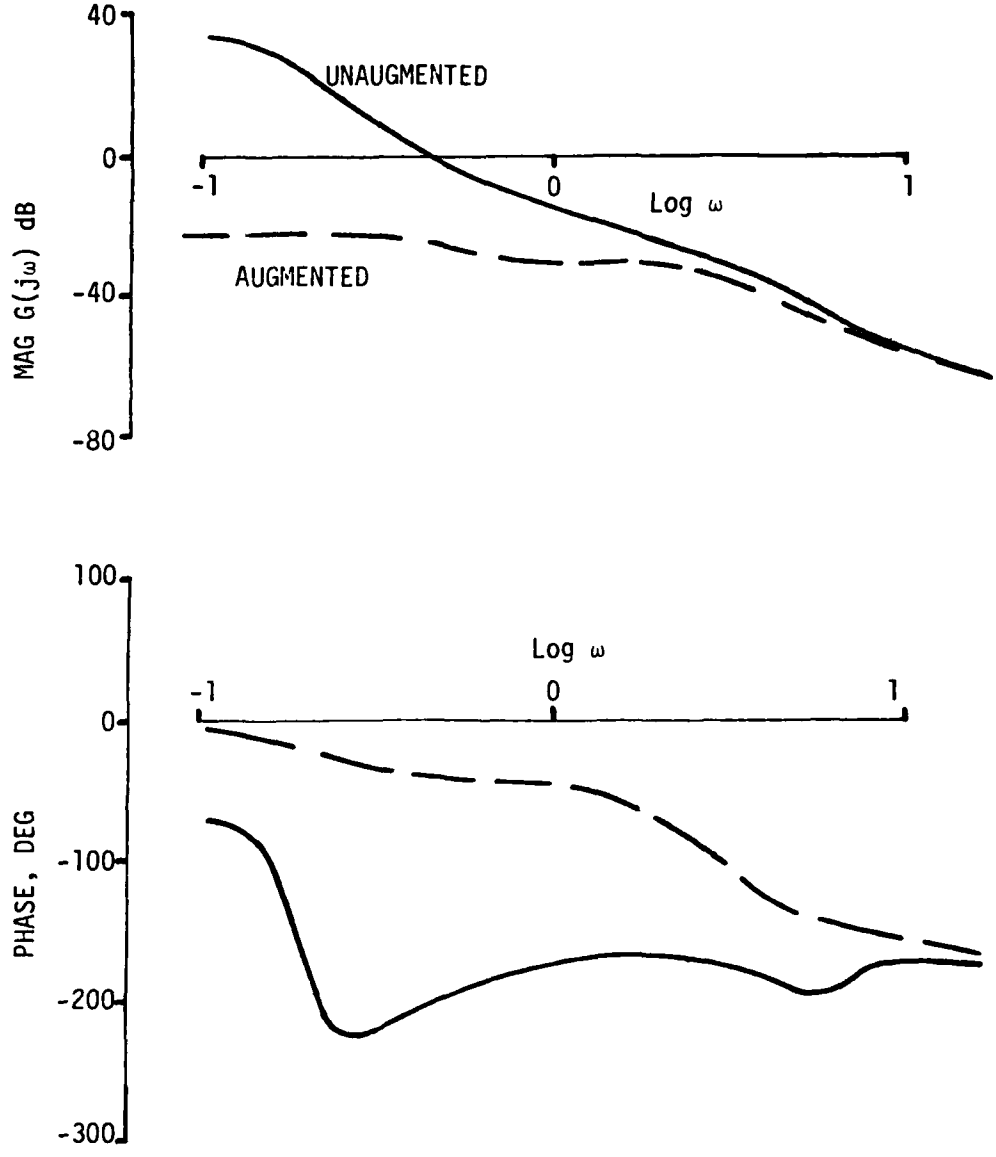

Fig. 17 Vehicle Describing Function $\varepsilon_{Az}/\delta_A$

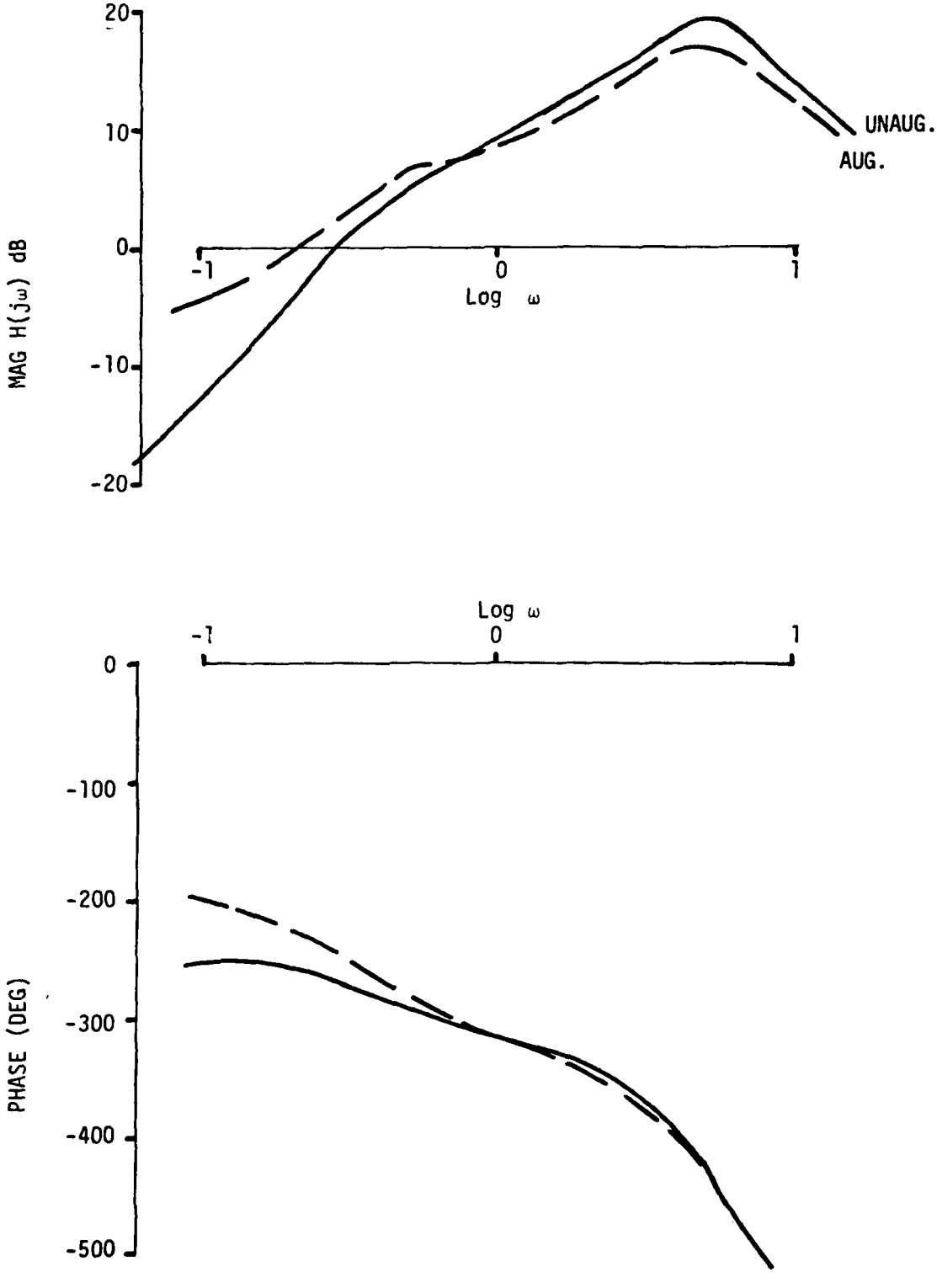

Fig. 18 Pilot's Describing Function δ_A/ϵ_{Az}

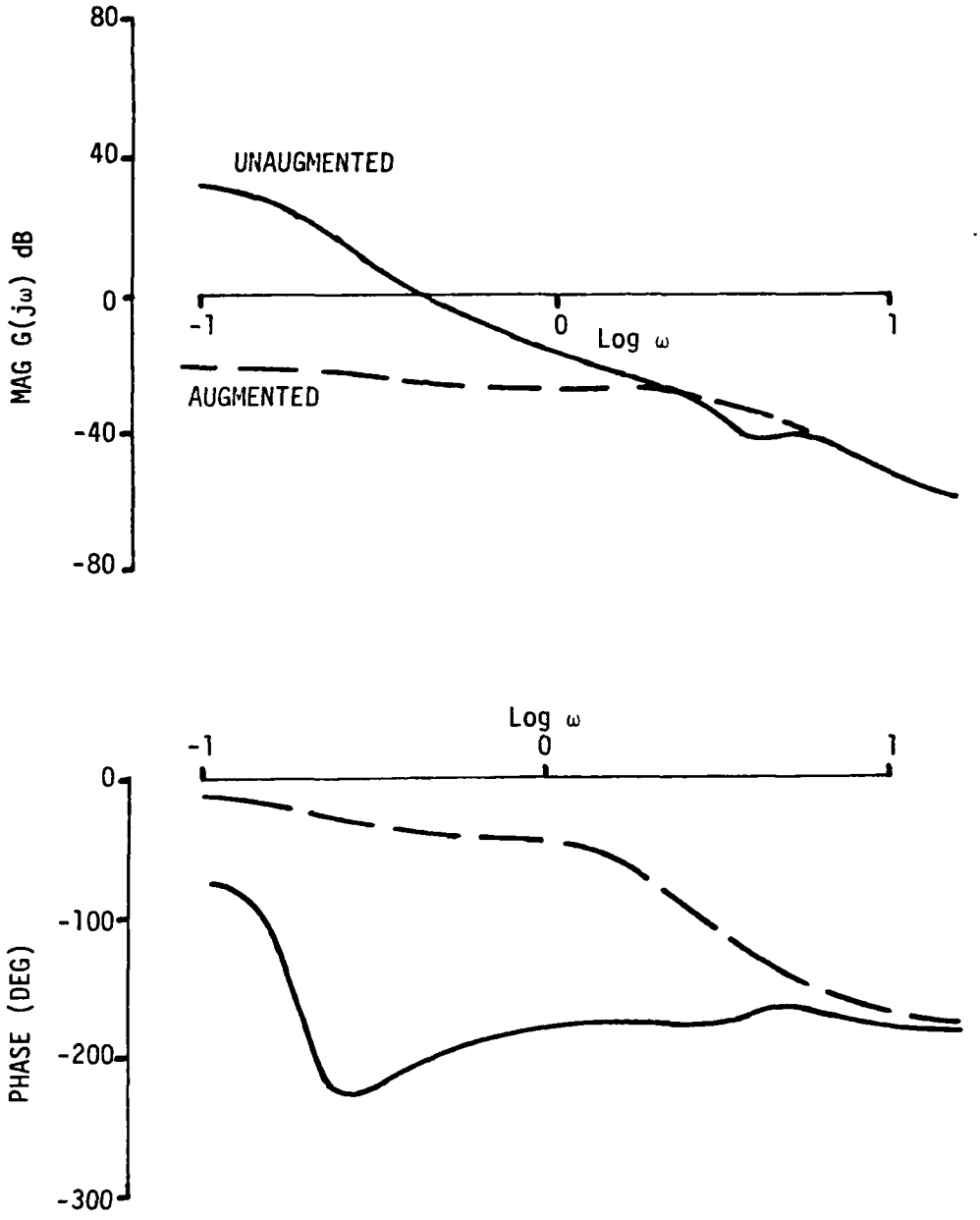

Fig. 19 Vehicle Describing Function $\varepsilon_{Az}/\delta_R$

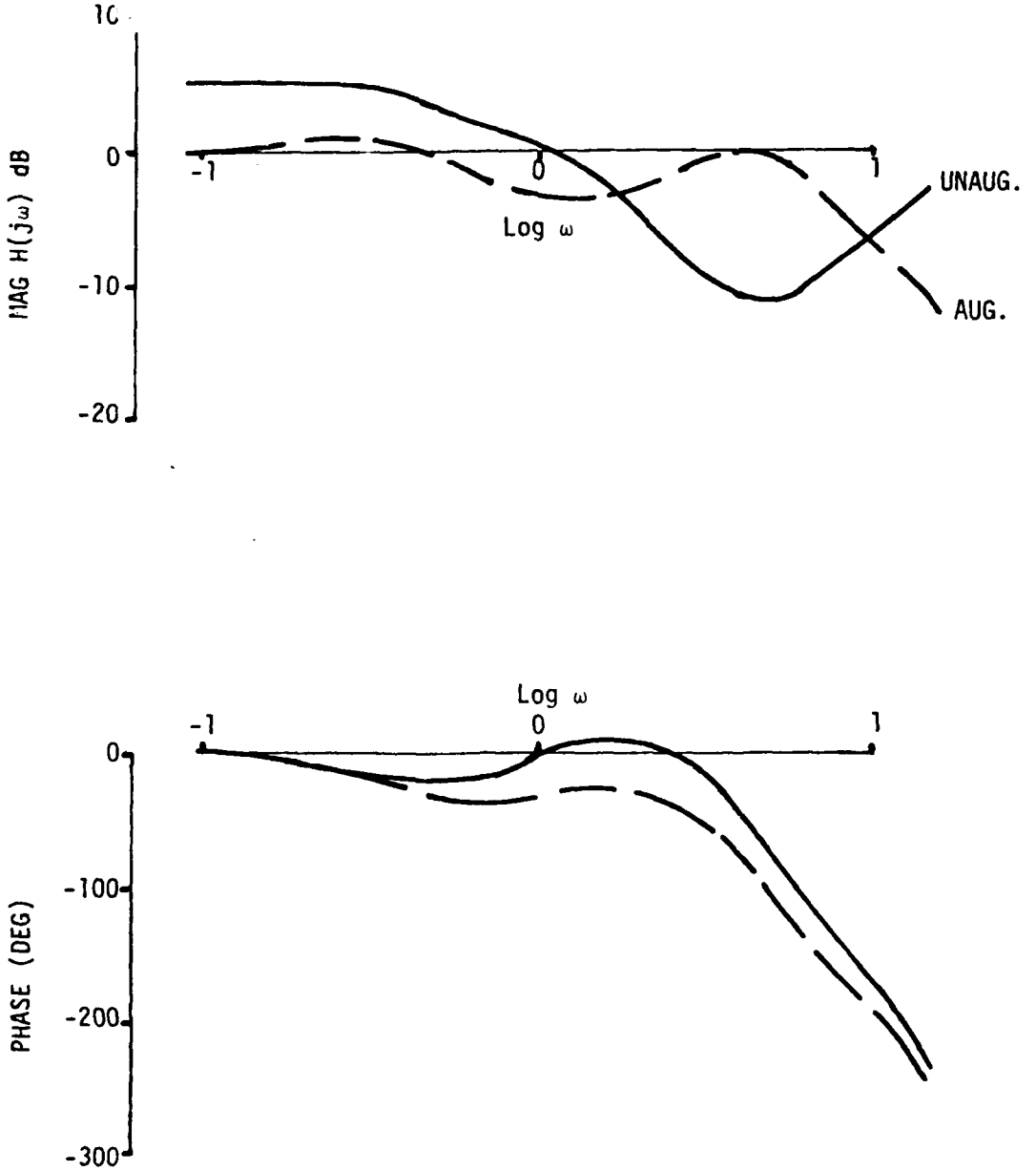

Fig. 20 Pilot's Describing Function $\delta_R/\varepsilon_{Az}$

Finally, the rudder frequency responses are shown in Figures 19 and 20. As with the aileron results, the pilot's rudder describing function indicates that the pilot is providing turn coordination and regulating azimuth error with rudder input.

To see the effects of the augmentation on the statistical performance, consider the results in Table 19. As anticipated, the rms tracking errors are reduced, and it is noted that the azimuth error has been reduced more than the elevation error. Since the lateral directional axis is considered the more difficult, it appears that the augmentation has significantly improved the tracking performance as predicted by linear analysis.

Note, finally, that the variance of the additive motor noise was the same for the augmented system analysis as for unaugmented. This results in a higher noise-to-signal ratio for the motor noise in the augmented case, and should yield conservative results for the performance predictions. In addition, the piloted predictions were made assuming the pilot used all three controls. However, the augmentation gains were determined using the assumption that no pilot rudder input would be used to reduce pilot workload (hence no gains on δ_R in Table 18). If no pilot rudder was actually evaluated, rms results would be further improved. Simulations are required in any future efforts to substantiate these results.

TABLE 19

AUGMENTED SYSTEM

RMS PERFORMANCE

	Tracking Errror (deg)		Lead Angles (deg)	
	ε_{El}	ε_{Az}	λ_{El}	λ_{Az}
Unaugmented	1.78	1.72	1.38	0.63
Augmented	0.54	0.20	0.33	0.10

	Target Velocities (ft/sec)		Euler Angles (deg)	
	w_T	v_T	θ	ϕ
Unaugmented	63.	25.	0.97	3.55
Augmented	15.	4.	0.17	0.48

	Velocity Angles (deg)		Angular Rates (deg/sec)		
	α	β	p	q	r
Unaugmented	0.97	0.15	5.21	2.58	0.57
Augmented	0.36	0.06	1.20	0.97	0.21

	Control Inputs (in)			Neuromotor Lags (sec)		
	$\delta_{E_{st}}$	$\delta_{A_{st}}$	$\delta_{R_{ped}}$	τ_{N_E}	τ_{N_A}	τ_{N_R}
Unaugmented	0.23	0.15	0.10	0.33	0.28	0.62
Augmented	0.19	0.11	0.06	0.33	0.28	0.62

	Lateral Accelerational (ft/sec^2)	Neuromotor Noise Ratios (dB)		
	a_y	N_{δ_E}	N_{δ_A}	N_{δ_R}
Unaugmented	0.78	-8.	-12.	-8.
Augmented	0.25	-7.	-8.	-4.

References

1. Schmidt, D.K., "Optimal Flight Control Synthesis Via Pilot Modeling," Journal of Guid. and Cont., Vol. 2, No. 4, July-Aug., 1979, pp. 308-312.

2. Anderson, R.O., "A New Approach to the Specification and Evaluation of Flying Qualities," AFFDL-TR-69-120, Wright-Patterson AFB, OH, December, 1969.

3. Harvey, T.R., "Application of an Optimal Control Pilot Model to Air-to-Air Combat," Air Force Institute of Technology M.S. Thesis, GA/MA/74M-1, Wright-Patterson AFB, OH, March, 1974.

4. Hollis, T.L., "Optimal Selection of Stability Augmentation System Parameters to Reduce the Pilot Ratings for the Pitch Tracking Task," Air Force Institute of Technology M.S. Thesis, GGC/EE/71-10, Wright-Patterson AFB, OH, June, 1971.

5. Kleinman, D.L., Baron, S., and Levison, W.H., "An Optimal Control Model of Human Response," Parts I and II, Automatica, Vol. 6, 1970, pp. 357-383.

6. Kwakernaak, H., and Sivan, R., Linear Optimal Control Systems, Sec. 3.8, Wiley and Sons, Inc., New York, 1972.

7. Levison, W.H., et. al.,"Studies of Multivariable Manual Control Systems: A Model For Task Interference," NASA CR-1746, May, 1971.

8. Harrington, W.W., Capt. "The Application of Pilot Modeling to the Study of Low Visibility Landing," Proceed. 12th Ann. Conf. on Man. Cont., Univ. of Ill., May, 1976.

9. Onstott, E.D., "Multi-Axis Pilot-Vehicle Dynamics," Proc. of the 10th Ann. Conf. on Manual Cont. Wright-Patterson AFB (AFIT), April, 1974.

10. Hess, R.A., "Prediction of Pilot Opinion Ratings Using an Optimal Pilot Model," Human Factors, Vol. 19, No. 5, October, 1977.

11. Levison, W.H. and Kleinman, D.L., "Analysis of Pilot/System Performance in Carrier Approach," Bolt, Beranek, and Newman, Inc., Cambridge, Mass., Sept., 1971.

12. Korn, J. and Kleinman, D.L., "Modeling Lateral Acceleration Effects on Pilot Performance in a Vectored Force Fighter," 16th Ann. Conf. on Manual Cont., MIT, Cambridge, Mass., May, 1980.

13. Curry, R.E., et. al., "Pilot Modeling for Manual Simulation," AFFDL-TR-76-124, Vols. I and II. Dec., 1976.

APPENDIX A

EQUATIONS FOR THE RELATIVE LINE OF SIGHT

Vector Equation Development

Clearly, the angle(s) to the line of sight (LOS) are required for our analysis, and as usual, linearized perturbation equations are ultimately required. The equations to be developed in this section will be derived for the angles, as shown in the figure below, in the vehicles gun coordinate system, X_g Y_g Z_g.

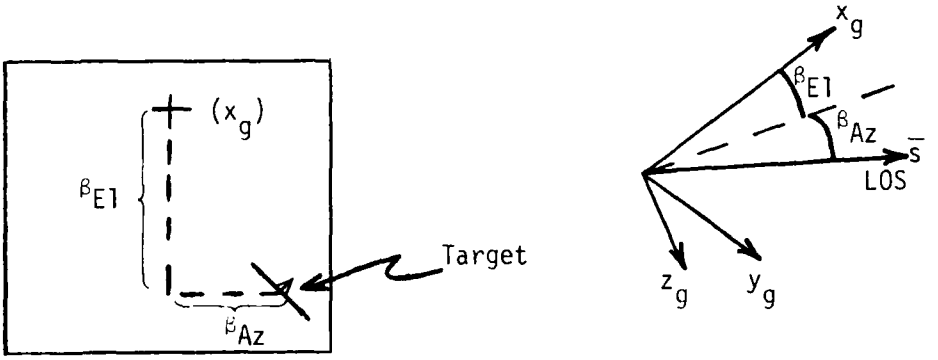

Heads-Up-Display Schematic

Now the kinematics of the line of sight unit vector, $\bar{s}$, are described by

$$\bar{V}_{Target} - \bar{V}_{Attacker} = \frac{d}{dt}(D\bar{s}) = \dot{D}\bar{s} + D\dot{\bar{s}} \qquad (A1)$$

where D is the scalar distance from the attacker to the target.

But the time rate of change of a unit vector is the cross product of that vector with its rate of rotation vector in inertial space, $\dot{\bar{\beta}}$, or

$$\dot{\bar{s}} = \dot{\bar{\beta}} \times \bar{s}$$

So $\dot{\bar{\beta}}$ is the rate of rotation of the LOS in the inertial (e.g. earth-fixed) coordinate system.

Taking the cross-product of Equation A1 with $\bar{s}$ yields

$$\bar{s} \times (\bar{V}_T - \bar{V}_A) = \bar{s} \times \dot{D}\bar{s} + \bar{s} \times (\dot{\bar{\beta}} \times \bar{s})\, D = D\bar{s} \times (\dot{\bar{\beta}} \times \bar{s})$$

And from the vector triple product identity

$$\bar{s} \times (\dot{\bar{\beta}} \times \bar{s}) = \dot{\bar{\beta}} - (\dot{\bar{\beta}} \cdot \bar{s})\, \bar{s}$$

Now, instead of the inertial LOS rate $\dot{\bar{\beta}}$, we desire the LOS rate in the attacker's gun coordinate system or $\dot{\bar{\beta}}_{gun}$, which is

$$\dot{\bar{\beta}}_{gun} = \dot{\bar{\beta}} - \bar{\omega}_g$$

where $\bar{\omega}_g$ in the rotation rate vector of the gun or aircraft system. Substituting into the above yields

$$\dot{\bar{\beta}}_{gun} + \bar{\omega}_g - [(\dot{\bar{\beta}}_{gun} + \bar{\omega}_g) \cdot \bar{s}]\bar{s} = \frac{1}{D}\, \bar{s} \times (\bar{V}_T - \bar{V}_A)$$

or

$$\dot{\bar{\beta}}_{gun} = \frac{1}{D}\, \bar{s} \times (\bar{V}_T - \bar{V}_A) - \bar{\omega}_g + (\dot{\bar{\beta}}_{gun} \cdot \bar{s})\bar{s} + (\bar{\omega}_g \cdot \bar{s})\bar{s}$$

Now the term $(\dot{\bar{\beta}}_{gun} \cdot \bar{s}) = 0$ since the rotation vector and the line of sight in the gun coordinate are orthogonal.

The necessary vector equation is then

$$\dot{\bar{\beta}}_{gun} = \frac{1}{D}[\bar{s} \times (\bar{V}_T - \bar{V}_A)] - \bar{\omega}_g + (\bar{\omega}_g \cdot \bar{s})\bar{s} \qquad \text{(A2)}$$

From the previous figure, we can define the vectors as follows, using small angle approximations

$$\bar{s} = \bar{i}_g + \beta_{Az}\bar{j}_g + \beta_{El}\bar{k}_g$$

$$\bar{\beta}_{gun} = -\beta_{El}\bar{j}_K + \beta_{Az}\bar{k}_g$$

$$\bar{\omega}_g = P_g\bar{i}_g + Q_g\bar{j}_g + R_g\bar{K}_g$$

$$\bar{V}_A = U_A\bar{i}_g + V_A\bar{j}_g + W_A\bar{k}_g$$

$$\bar{V}_T = U_{T_g}\bar{i}_g + V_{T_g}\bar{j}_g + W_{T_g}\bar{k}_g$$

(It's important to note that $\bar{V}_T$ and the components here defined are the velocity components of the target in the attacker's gun coordinate system.) Carrying out the operations in Equation A2, and assuming $\bar{\omega}_g \cdot \bar{s} \simeq P_g$, we have the desired relations

$$\dot{\beta}_{El} = \frac{1}{D}\left[(W_{T_g} - W_g) - \beta_{El}(U_{T_g} - U_g)\right] + Q_g - P_g\beta_{Az}$$

$$\dot{\beta}_{Az} = \frac{1}{D}\left[(V_{T_g} - V_g) - \beta_{Az}(U_{T_g} - U_g)\right] - R_g + P_g\beta_{El}$$

To obtain the equation for the rate of change of range, or $\dot{D}$, we can simply take the dot product of Equation A1 with $\bar{s}$ to obtain

$$(\bar{V}_T - \bar{V}_A) \cdot \bar{s} = \dot{D}(\bar{s} \cdot \bar{s}) + D(\dot{\bar{\beta}} \times \bar{s}) \cdot \bar{s}$$

so

$$\dot{D} = (\bar{V}_T - V_A) \cdot \bar{s}$$

$$\dot{D} = (U_{T_g} - U_g) + (V_{T_g} - V_g)\beta_{Az} + (W_{T_g} - W_g)\beta_{El}$$

Scalor Equations in Stability Axes

Since all our equations are ultimately expressed in the vehicle stability axes, we need to express the above equations in terms of stability-axes variables rather than gun-coordinate variables.

Assuming the gun axis to be aligned with the vehicle body reference axis, we have the following relations between gun $(\cdot)_g$ and stability $(\cdot)_s$ variables

$$U_g = U_s \cos\alpha_1 - W_s \sin\alpha_1$$

$$V_g = V_s$$

$$W_g = W_s \cos\alpha_1 + U_s \sin\alpha_1$$

$$P_g = P_s \cos \alpha_1 - R_s \sin \alpha_1$$

$$Q_g = Q_s$$

$$R_g = R_s \cos \alpha_1 + P_s \sin \alpha_1$$

The resulting equations are

$$\begin{aligned}
\dot{D} &= [(U_{T_s} - U_s) \cos \alpha_1 - (W_{T_s} - W_s) \sin \alpha_1] \\
&\quad + \beta_{Az}(V_{T_s} - V_s) \\
&\quad + \beta_{El}[(W_{T_s} - W_s) \cos \alpha_1 + (U_{T_s} - U_s) \sin \alpha_1] \\
\dot{\beta}_{El} &= \frac{1}{D}[(W_{T_s} - W_s) \cos \alpha_1 + (U_{T_s} - U_s) \sin \alpha_1 \\
&\quad - \beta_{El}\{(U_{T_s} - U_s) \cos \alpha_1 - (W_{T_s} - W_s) \sin \alpha_1\}] \\
&\quad + Q_s - \beta_{Az}(P_s \cos \alpha_1 - R_s \sin \alpha_1) \\
\dot{\beta}_{Az} &= \frac{1}{D}[(V_{T_s} - V_s) - \beta_{Az}\{(U_{T_s} - U_s) \cos \alpha_1 - (W_{T_s} - W_s)\sin \alpha_1\}] \\
&\quad - (R_s \cos \alpha_1 + P_s \sin \alpha_1) + \beta_{EL}(P_s \cos \alpha_1 - R_s \sin \alpha_1)
\end{aligned} \tag{A3}$$

where U_{T_s}, V_{T_s}, W_{T_s} are now the components of the target velocity in the attacker's stability axis and α_1 is the attacker's trim angle of attack (or the trim angle between the gun axis and stability axis).

The Perturbation Equation

Now to linearize the above equations, we will define the motion variables in terms of a constant, steady-state quantity $(\cdot)_1$ and a time-varying perturbation about the steady-state variable. So, let

$$D = D_1 + d \qquad U_s = U_1 + u \qquad P_s = P_1 + p$$

$$\beta_{EL} = B_{EL_1} + \beta_{El} \qquad V_s = V_1 + v \qquad Q_s = Q_1 + q$$

$$\beta_{Az} = B_{Az_1} + \beta_{A_z} \qquad W_s = W_1 + w \qquad R_s = R_1 + r$$

Inserting these into Equations A3 will yield two sets of equations, one for the steady state values and one for the perturbation quantities. For example, taking the $\dot{\beta}_{E1}$ equation we have

$$(D_1 + d)(\dot{B}_{E1_1} + \dot{\beta}'_{E1}) = [(W_{T_1} - W_1)\cos\alpha_1 + (U_{T_1} - U_1)\sin\alpha_1]$$

$$+[(w_T - w)\cos\alpha_1 + (u_T - u)\sin\alpha_1]$$

$$-(B_{E1_1} + \beta'_{E1})[(U_{T_1} - U_1)\cos\alpha_1 - (W_{T_1} - W_1)\sin\alpha_1 \quad \text{(A4)}$$

$$+(u_T - u)\cos\alpha_1 - (w_T - w)\sin\alpha_1]$$

$$+ (D_1 + d)(Q_1 + q)$$

$$- (D_1 + d)(B_{Az_1} + \beta'_{Az})[(P_1 + p)\cos\alpha_1 - (R_1 + r)\sin\alpha_1]$$

Now the steady state $(\cdot)_1$ values certainly must obey the original equation, so

$$D_1\dot{B}_{E1_1} = 0 = [(W_{T_1} - W_1)\cos\alpha_1 + (U_{T_1} - U_1)\sin\alpha_1]$$

$$- B_{E1_1}[(U_{T_1} - U_1)\cos\alpha_1 - (W_{T_1} - W_1)\sin\alpha_1]$$

$$+ D_1Q_1 - D_1 B_{Az_1}[P_1\cos\alpha_1 - R_1\sin\alpha_1]$$

We may, as a result, subtract this relation out of the complete, original relation (Eqn A4). In addition, under the assumption that the perturbation variables are small, we will drop higher order terms (e.g., products of perturbation quantities). Finally, noting that $\dot{B}_{EL_1} = 0$ by definition, we have

$$D_1\dot{\beta}'_{E1} = [(w_T - w)\cos\alpha_1 + (u_T - u)\sin\alpha_1]$$

$$- B_{E1_1}[(u_{T_1} - u)\cos\alpha_1 - (w_{T_1} - w)\sin\alpha_1]$$

$$- \beta'_{E1}[(U_T - U_1)\cos\alpha_1 - (W_T - W_1)\sin\alpha_1] \quad \text{(cont'd)}$$

$$+ D_1 q + Q_1 d - d\, B_{Az_1} (P_1 \cos\alpha_1 - R_1 \sin\alpha_1)$$
$$- \beta'_{Az} D_1 (P_1 \cos\alpha_1 - R_1 \sin\alpha_1) - D_1 B_{Az_1} (p \cos\alpha_1 - r \sin\alpha_1)$$

This equation is now linear in terms of the perturbation variables, and the steady-state variables are constant by definition.

In like manner, the remaining two equations in A3 result in

$$\dot{D}_1 = 0 = [(U_{T_1} - U_1)\cos\alpha_1 - (W_{T_1} - W_1)\sin\alpha_1] + B_{Az}(V_{T_1} - V_1)$$
$$+ B_{E1}[(W_{T_1} - W_1)\cos\alpha_1 + (U_{T_1} - U_1)\sin\alpha_1]$$
$$\dot{d} = [(u_T - u)\cos\alpha_1 - (w_T - w)\sin\alpha_1] + \beta'_{Az}(V_{T_1} - V_1)$$
$$+ B_{Az_1}(v_T - v) + \beta'_{E1}[(W_{T_1} - W_1)\cos\alpha_1 + (U_{T_1} - U_1)\sin\alpha_1]$$
$$+ B_{E1_1}[(w_T - w)\cos\alpha_1 + (u_T - u)\sin\alpha_1]$$
$$\dot{B}_{Az_1} = 0 = \frac{1}{D_1}[(V_{T_1} - V_1) - B_{Az}\{(U_{T_1} - U_1)\cos\alpha_1 - (W_{T_1} - W_1)\sin\alpha_1\}]$$
$$-(R_1 \cos\alpha_1 + P_1 \sin\alpha_1) + B_{E1_1}(P_1 \cos\alpha_1 - R_1 \sin\alpha_1)$$

and
$$D_1 \dot{\beta}'_{Az} = (v_T - v) - B_{Az_1}[(u_T - u)\cos\alpha_1 - (w_T - w)\sin\alpha_1]$$
$$-\beta'_{Az}[(U_{T_1} - U_1)\cos\alpha_1 - (W_{T_1} - W_1)\sin\alpha_1]$$
$$-D_1 (r \cos\alpha_1 + p \sin\alpha_1) - d\,(R_1 \cos\alpha_1 + P_1 \sin\alpha_1)$$
$$+D_1 B_{E1_1}(p \cos\alpha_1 - r \sin\alpha_1) + D_1 \beta'_{E1}(P_1 \cos\alpha_1 - R_1 \sin\alpha_1)$$
$$+ d\, B_{E1_1}(P_1 \cos\alpha_1 - R_1 \sin\alpha_1)$$

APPENDIX B

EQUATIONS FOR THE SIGHT LEAD ANGLES

Perfect Director

Again, linearized equations are needed for the lead angles computed by the sights. From the reference*, the fundamental equation for the lead angle, $\bar{\lambda}$, in general, is

$$V_f\bar{\lambda} = \bar{s} \times (\bar{V}_T - \bar{V}_A) + J_V V_A \bar{\alpha}_{gun} + (\bar{s} \times \dot{\bar{V}}_T)\frac{T_f}{2} \qquad (B1)$$

where, referring to the figure and assuming the sight (pipper) is on the target, we have

$$\bar{s} = \bar{i}_g + \lambda_{Az}\bar{j}_g + \lambda_{El}\bar{K}_g$$

or

$$\bar{s} = i_g + \beta_{Az}\bar{j}_g + \beta_{El}\bar{K}_g$$

$$\bar{\lambda} = \bar{s} \times \bar{i}_{gun} = \lambda_{El}\bar{j}_{gun} - \lambda_{Az}\bar{k}_{gun}$$

V_f = average projectile velocity in still air

($V_f = D_f/T_f - V_A$, D_f = distance of flight)

T_f = projectile time of flight

V_A = attacker's velocity

J_V = Jump correction factor, $= \frac{V_M - V_f}{V_A + V_M}$, V_M is projectile muzzle velocity

$\bar{\alpha}_{gun} = \bar{i}_{gun} \times \frac{\bar{V}_A}{|\bar{V}_A|} = -\alpha\bar{j}_{gun} + \beta k_{gun}$, α and β here are angle of attack and sideslip

$\dot{\bar{V}}_T$ = target's acceleration

*Hohwiesner, W., Capt. "Principles of Airborne Fire Control," USAF Academy, Dept. of Astro. and Comp. Sci., Dec. 1975.

To obtain the scalar component equations, define the following vectors in the gun coordinate system

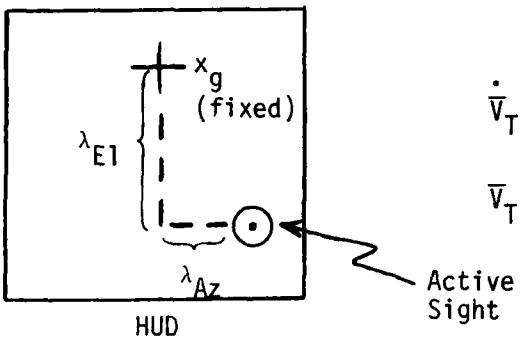

$$\dot{\bar{V}}_T = A_{T_x}\bar{i}_{gun} + A_{T_y}\bar{j}_{gun} + A_{T_z}\bar{k}_{gun}$$

$$\bar{V}_T = U_{T_g}\bar{i}_{gun} + V_{T_g}\bar{j}_{gun} + W_{T_g}k_{gun}$$

where as in the LOS equation development, it's important to remember that the target's velocity and acceleration components are in the attacker's gun coordinate system. Carrying out the vector operation yields

$$V_f\lambda_{El} = [\beta_{El}(U_{T_g} - U_g) - (W_{T_g} - W_g)] - J_V V_A\alpha + (\beta_{El}A_{T_{X_g}} - A_{T_{Z_g}})\frac{T_f}{2}$$

$$-V_f\lambda_{Az} = [(V_{T_g} - V_g) - \beta_{Az}(U_{T_g} - U_g)] + J_V V_A\beta + (A_{T_{Y_g}} - \beta_{Az}A_{T_{Y_g}})\frac{T_f}{2}$$

These equations may be used to calculate lead angles assuming the actual line-of-sight angles (β's) and target acceleration are known. This ideal case is referred to as a perfect director sight.

Now, these equations will be expressed in terms of stability axis velocities, etc. rather than gun axis. We have the relations

$$U_g = U_s \cos \alpha_1 - W_s \sin \alpha_1$$

$$V_g = V_s$$

$$W_g = W_s \cos \alpha_1 + U_s \sin \alpha_1$$

$$A_{T_{X_g}} = A_{T_{X_s}} \cos \alpha_1 - A_{T_{Z_s}} \sin \alpha_1$$

$$A_{T_{Y_g}} = A_{T_{Y_s}}$$

$$A_{T_{Z_g}} = A_{T_{Z_s}} \cos \alpha_1 + A_{T_{X_s}} \sin \alpha_1$$

Finally, using the perturbation technique employed in the previous appendix we introduce the relation

$$\lambda_{E1} = L_{E1} + \lambda'_{E1} \qquad A_{T_{X_s}} = A_{T_{X_1}} + a_{t_x}$$

$$\alpha = \alpha_1 + \alpha' \qquad \text{etc.}$$

Introducing these perturbations and assuming that V_f, T_f, and J_V are constant for this analysis we have the following steady state relations

$$V_f L_{E1} = B_{E1}[(U_{T_1} - U_1) \cos \alpha_1 - (W_{T_1} - W_1) \sin \alpha_1]$$
$$-[(W_{T_1} - W_1) \cos \alpha_1 + (U_{T_1} - U_1) \sin \alpha_1]$$
$$-J_v V_{A_1} \alpha_1 - \frac{T_f}{2}[(A_{T_{Z_1}} \cos \alpha_1 + A_{T_{X_1}} \sin \alpha_1$$
$$-B_{E1}(A_{T_{X_1}} \cos \alpha_1 - A_{T_{Z_1}} \sin \alpha_1]$$

and

$$-V_f L_{Az} = (V_{T_1} - V_1) - B_{Az}[(U_{T_1} - U_1) \cos \alpha_1 - (W_{T_1} - W_1) \sin \alpha_1]$$
$$+ J_V V_A \beta_1 + \frac{T_f}{2}[A_{T_{Y_1}} - B_{Az}(A_{T_{X_1}} \cos \alpha_1 - A_{T_{Z_1}} \sin \alpha_1]$$

Furthermore the perturbation equations are

$$V_f \lambda'_{El} = B_{El}[(u_T - u)\cos\alpha_1 - (w_T - w)\sin\alpha_1]$$
$$+ \beta'_{El}[(U_{T_1} - U_1)\cos\alpha_1 - (W_{T_1} - W_1)\sin\alpha_1]$$
$$- [(w_T - w)\cos\alpha_1 + (u_T - u)\sin\alpha_1]$$
$$-\frac{T_f}{2}(a_{T_z}\cos\alpha_1 + a_{T_x}\sin\alpha_1)$$
$$- B_{El}(a_{T_x}\cos\alpha_1 - a_{T_z}\sin\alpha_1)$$
$$- \beta'_{El}(A_{T_{X_1}}\cos\alpha_1 - A_{T_{Z_1}}\sin\alpha_1)$$
$$- J_V V_A \alpha'$$

and

$$-V_f \lambda'_{Az} = (v_T - v) - B_{Az}[(u_T - u)\cos\alpha_1 - (w_T - w)\sin\alpha_1]$$
$$-\beta'_{Az}[(U_{T_1} - U_1)\cos\alpha_1 - (W_{T_1} - W_1)\sin\alpha_1]$$
$$+ \frac{T_f}{2}[a_{T_Y} - B_{Az}(a_{T_x}\cos\alpha_1 - a_{T_z}\sin\alpha_1)$$
$$-\beta'_{Az}(A_{T_{x_1}}\cos\alpha_1 - A_{T_{z_1}}\sin\alpha_1)]$$
$$+ J_V V_A \beta'$$

LCOS Equation

Returning to equation B1 in the previous section, recall that the perfect director assumes perfect knowledge of the line-of-sight rate and target acceleration. The lead computing optical sight (LCOS) system, however, uses attacker rotation rates and acceleration to approximate the above parameters.

In terms of the line of sight rate in the attacker's gun coordinate system, $\dot{\bar{\beta}}_{gun}$ we have from the cited reference,as well as the previous appendix,

$$\dot{\bar{\beta}} = \bar{\omega}_g + \dot{\bar{\beta}}_{gun}$$

but, the $\bar{\lambda}$ vector defined here is used as an approximation for $-\beta_{gun}$ for the LCOS, and where the $\bar{\beta}$ vector is defined in the previous appendix.

In this case then,

$$\dot{\bar{\beta}} \tilde{=} \bar{\omega}_g - \dot{\bar{\lambda}}$$

Now since as shown in previous appendix

$$\bar{s} \times (\bar{V}_T - \bar{V}_A) = D[\dot{\bar{\beta}} - (\bar{\beta} \cdot \bar{s})\, \bar{s}]$$

and

$$\dot{\bar{\beta}} - (\dot{\bar{\beta}} \cdot \bar{s})\bar{s} \tilde{=} (\bar{\omega}_g - \dot{\bar{\lambda}}) - [(\bar{\omega}_g - \dot{\bar{\lambda}}) \cdot \bar{s}]\bar{s}$$

so

$$\bar{s} \times (\bar{V}_T - \bar{V}_A) \tilde{=} (\bar{\omega}_g - \dot{\bar{\lambda}}) - (\bar{\omega}_g \cdot \bar{s})\bar{s} + (\dot{\bar{\lambda}} \cdot \bar{s})\bar{s}$$

In addition, the attacker acceleration $\bar{A}_A$ is substituted in place of the target's, resulting in the vector equation for the LCOS (with $\dot{\bar{\lambda}} \cdot \bar{s}$ equal zero)

$$V_f \bar{\lambda} = D[(\bar{\omega}_g - \dot{\bar{\lambda}}) - (\bar{\omega}_g \cdot \bar{s})\, \bar{s}\,] + J_V V_A \bar{\alpha}_{gun} + (\bar{s} \times \bar{A}_A)\, \frac{T_f}{2}$$

so, with

$$\bar{s} = i_g + \lambda_{Az} j_g + \lambda_{EL} \bar{k}_g$$

$$\bar{\omega}_g = P_g \bar{i}_g + Q_g \bar{j}_g + R_g \bar{k}_g$$

and $$\bar{A}_A = A_x \bar{i}_g + A_y \bar{j}_g + A_z \bar{k}_g$$

we have the following two scalar differential equations

$$\dot{D\lambda}_{EL} = -V_f\lambda_{EL} + DQ_g - D(P_g + \lambda_{Az}Q_g + \lambda_{EL}R_g)\lambda_{Az}$$

$$-J_vV_A\alpha + \frac{T_f}{2}(\lambda_{El}A_x - A_z)$$

and $$-\dot{D\lambda}_{Az} = V_f\lambda_{Az} + D\,R_g - D(P_g + \lambda_{Az}\,Q_g + \lambda_{EL}\,R_g)\,\lambda_{EL}$$

$$+J_vV_A\beta + \frac{T_f}{2}(A_y - \lambda_{Az}A_x)$$

The steady state equations are then, using the usual perturbation technique,

$$\dot{D_1L}_{EL} = 0 = -V_fL_{Az} + D_1Q_1 - J_vV_A\alpha_1$$

$$+ \frac{T_f}{2}[L_{EL}(A_{x_1}\cos\alpha_1 - A_{z_1}\sin\alpha_1) - (A_{z_1}\cos\alpha_1 + A_{x_1}\sin\alpha_1)]$$

$$- D_1L_{Az}[(P_1\cos\alpha_1 - R_1\sin\alpha_1) + L_{Az}Q_1 + L_{EL}(R_1\cos\alpha_1 + P_1\sin\alpha_1)]$$

$$-\dot{D_1L}_{Az} = 0 = V_fL_{Az} + D_1(R_1\cos\alpha_1 + P_1\sin\alpha_1)$$

$$+ J_vV_A\beta_1 + \frac{T_f}{2}[A_{y_1} - L_{Az}(A_{x_1}\cos\alpha_1 - A_{z_1}\sin\alpha_1)]$$

$$-D_1L_{EL}[(P_1\cos\alpha_1 - R_1\sin\alpha_1) + L_{Az}Q_1 + L_{EL}(R_1\cos\alpha_1 + P_1\sin\alpha_1)]$$

Finally, the perturbation equations become

$$\dot{D_1\lambda'_{EL}} = -V_f\lambda'_{E1} + D_1q + Q_1d - J_vV_A\alpha'$$

$$+ \frac{T_f}{2}[L_{EL}(a_x\cos\alpha_1 - a_z\sin\alpha_1)$$

$$+ \lambda'_{E1}(A_{x_1}\cos\alpha_1 - A_{z_1}\sin\alpha_1) \quad \text{(cont'd)}$$

$$- (a_z \cos \alpha_1 + a_x \sin \alpha_1)]$$

$$- dL_{AZ} M_1 - D_1 \dot{\lambda}_{Az} M_1$$

$$- D_1 L_{AZ}[(p \cos \alpha_1 - r \sin \alpha_1) + \lambda_{Az} Q_1 + L_{Az} q$$

$$+ \lambda_{E1}(R_1 \cos \alpha_1 + P_1 \sin \alpha_1)$$

$$+ L_{EL}(r \cos \alpha_1 + p \sin \alpha_1)]$$

$$-D_1 \dot{\lambda}_{Az} = V_f \lambda_{Az} + D_1(r \cos \alpha_1 + p \sin \alpha_1)$$

$$+ d(R_1 \cos \alpha_1 + P_1 \sin \alpha_1) + J_v V_A \beta$$

$$+ \frac{T_f}{2}[a_y - \lambda_{Az}(A_{x_1} \cos \alpha_1 - A_{z_1} \sin \alpha_1)$$

$$- L_{A_z}(a_x \cos \alpha_1 - a_z \sin \alpha_1)]$$

$$- dL_{EL} M_1 - D_1 \lambda_{E1} M_1$$

$$- D_1 L_{EL}[(p \cos \alpha_1 - r \sin \alpha_1) + L_{AZ} q + \lambda_{Az} Q_1$$

$$+ \lambda_{EL}(R_1 \cos \alpha_1 + P_1 \sin \alpha_1) + L_{EL}(r \cos \alpha_1 + p \sin \alpha_1)]$$

where in the above relations

$$M_1 = (P_1 \cos \alpha_1 - R_1 \sin \alpha_1) + L_{Az} Q_1$$

$$+ L_{EL}(R_1 \cos \alpha_1 + P_1 \sin \alpha_1)$$

APPENDIX C

TARGET KINEMATICS

In the foregoing appendices, the equations for the line-of-sight rates and sight lead angles were developed in terms of the attacker's velocities and of the target's velocities expressed in the attacker coordinate system. In this appendix, the relations governing these target kinematics will be developed.

Consider the target's velocity vector expressed in the attacker's gun coordinates as

$$\bar{V}_T = U_T \bar{i}_A + V_T \bar{j}_A + W_T \bar{k}_A$$

Now, the time rate of change of this vector with respect to the attacker's coordinates is simply

$$\dot{\bar{V}}_T\Big|_A = \dot{U}_T \bar{i}_A + \dot{V}_T \bar{j}_A + \dot{W}_T \bar{k}_A$$

But we may also express this acceleration vector in terms of the time rate of change of the target's velocity vector relative to the target's own coordinate system, plus the effect of the relative motion between the two coordinate systems,

or

$$\dot{\bar{V}}_T\Big|_A = \dot{\bar{V}}\Big|_T + \bar{\omega}_{rel} \times \bar{V}_T \qquad (C1)$$

where $\dot{\bar{V}}\Big|_T = \dot{U}_{T_T} \bar{i}_T + \dot{V}_{T_T} \bar{j}_T + \dot{W}_{T_T} \bar{k}_T$

Here, then, $\bar{\omega}_{rel}$ is the rate of rotation of the target's coordinate system relative to the attacker's, or in terms of the two aircraft angular rates relative to inertial coordinates

$$\bar{\omega}_{rel} = \bar{\omega}_T - \bar{\omega}_A$$

$$\bar{\omega}_T = P_T \bar{i}_T + Q_T \bar{j}_T + R_T \bar{k}_T$$

$$\bar{\omega}_A = P_A \bar{i}_A + Q_A \bar{j}_A + R_A \bar{k}_A$$

Finally, the relative orientation of the two coordinate systems is required to allow coordinate transformation of vectors. This may be accomplished in terms of the usual Euler angles Θ, ψ , and ϕ for each vehicle where

ψ = inertial heading angle

Θ = angle of elevation above local horizontal

ϕ = roll angle

Let

$$T(\Theta) = \begin{bmatrix} \cos\Theta & 0 & \sin\Theta \\ 0 & 1 & 0 \\ -\sin\Theta & 0 & \cos\Theta \end{bmatrix}$$

$$T(\psi) = \begin{bmatrix} \cos\psi & -\sin\psi & 0 \\ \sin\psi & \cos\psi & 0 \\ 0 & 0 & 1 \end{bmatrix}$$

$$T(\phi) = \begin{bmatrix} 1 & 0 & 0 \\ 0 & \cos\phi & -\sin\phi \\ 0 & \sin\phi & \cos\phi \end{bmatrix}$$

Then, noting that $T^{-1}(a) = T^T(a) = T(-a)$, we can express $\dot{\bar{V}}\Big|_T$ and $\bar{\omega}_T$ in terms of their components in the attacker's coordinates, since

$$\begin{pmatrix} \bar{i}_T \\ \bar{j}_T \\ \bar{k}_T \end{pmatrix} = T(-\phi_T)\ T(-\Theta_T)\ T(-\psi_T)\ T(\psi_A)\ T(\Theta_A)\ T(\phi_A) \begin{pmatrix} \bar{i}_A \\ \bar{j}_A \\ \bar{k}_A \end{pmatrix}$$

After determining these components we can obtain the vectors

$$\dot{\bar{V}}\Big|_T = \dot{U}_{T_T}\, \bar{i}_A + \dot{V}_{T_T}\, \bar{j}_A + \dot{W}_{T_T}\, \bar{K}_A$$

$$\bar{\omega}_T = P_T'\, \bar{i}_A + Q_T'\, \bar{j}_A + R_T'\, \bar{K}_A$$

So we may write

$$\bar{\omega}_{rel} = (P_T' - P_A)\, \bar{i}_A + (Q_T' - Q_A)\, \bar{j}_A + (R_T' - R_A)\, \bar{K}_A$$

or $$\bar{\omega}_{rel} = P_{rel}\, \bar{i}_A + Q_{rel}\, \bar{j}_A + R_{rel}\, \bar{K}_A$$

Therefore, we obtain the resulting desired relations governing the target's motion in attacker's coordinates from Equation C1

$$\dot{U}_T = \dot{U}_{T_T} + W_T\, Q_{rel} - V_T\, R_{rel}$$

$$\dot{V}_T = \dot{V}_{T_T} + U_T\, R_{rel} - W_T\, P_{rel}$$

$$\dot{W}_T = \dot{W}_{T_T} + V_T\, P_{rel} - U_T\, Q_{rel}$$

Defining the above quantities in terms of steady state and perturbation quantities yields the steady-state equations

$$\dot{U}_{T_1} = \dot{U}_{T_{T_1}} + W_{T_1}\, Q_{rel_1} - V_{T_1}\, R_{rel_1}$$

$$\dot{V}_{T_1} = \dot{V}_{T_{T_1}} + U_{T_1}\, R_{rel_1} - W_{T_1}\, P_{rel_1}$$

$$\dot{W}_{T_1} = \dot{W}_{T_{T_1}} + V_{T_1}\, P_{rel_1} - U_{T_1}\, Q_{rel_1}$$

Here note that $\dot{U}_{T_{T_1}} = \dot{V}_{T_{T_1}} = \dot{W}_{T_{T_1}} = 0$ since the steady-state target velocity is constant in the target coordinate system. The above relations also show the required conditions for the target steady-state velocity to be constant in the attacker's coordinate system as well.

AD-A090 050 PURDUE UNIV LAFAYETTE IND SCHOOL OF AERONAUTICS AND --ETC F/G 5/8
MULTIVARIABLE CLOSED-LOOP ANALYSIS AND FLIGHT CONTROL SYNTHESIS--ETC(U)
JUN 80 D K SCHMIDT AFOSR-79-0042

UNCLASSIFIED AFOSR-TR-80-0961 NL

2 OF 2

END
DATE FILMED
11-80
DTIC

These conditions are

$$W_{T_1} Q_{rel_1} = V_{T_1} R_{rel_1}$$

$$U_{T_1} R_{rel_1} = W_{T_1} P_{rel_1}$$

$$V_{T_1} P_{rel_1} = U_{T_1} Q_{rel_1}$$

Finally, the perturbation equations for the target's velocity components in the attacker's coordinates are

$$\dot{u}_T = \dot{u}'_{T_T} + W_{T_1} q_{rel} + w_T Q_{rel_1}$$
$$- V_{T_1} r_{rel} - v_T R_{rel_1}$$

$$\dot{v}_T = \dot{v}'_{T_T} + U_{T_1} r_{rel} + u_T R_{rel_1}$$
$$-W_{T_1} p_{rel} - w_T P_{rel_1}$$

$$\dot{w}_T = \dot{w}'_{T_T} + V_{T_1} p_{rel} + v_T P_{rel_1}$$
$$-U_{T_1} q_{rel} - u_T Q_{rel_1}$$

Now if the target is simply in a steady flight condition, note that the target's perturbation acceleration terms $\dot{u}'_{T_T} = \dot{v}'_{T_T} = \dot{w}'_{T_T} = 0$.

APPENDIX D

F106 PERTURBATION EQUATIONS

In this section, the linearized equations for the vehicle dynamics are summarized. From the reference* the perturbation equations for a general steady-state flight condition are as follows:

$$\dot{u} - V_1 r - R_1 v + W_1 q + Q_1 w = -g\theta\cos\Theta_1 + X_u u + X_w w + X_{\delta_E}\delta_E$$

$$\dot{v} + U_1 r + R_1 u - W_1 p - P_1 w = -g\theta\sin\Phi_1 \sin\Theta_1 + g\phi\cos\Phi_1 \cos\Theta_1 + Y_v v + Y_p p + Y_r r + Y_{\delta_A}\delta_A + Y_{\delta_R}\delta_R$$

$$\dot{w} - U_1 q - Q_1 u + V_1 p + P_1 v = -g\theta\cos\Phi_1 \sin\Theta_1 - g\phi\sin\Phi_1 \cos\Theta_1 + Z_u u + Z_w w + Z_{\delta_E}\delta_E$$

$$\dot{q} + \frac{1}{I_{yy}}(I_{xx} - I_{zz})(P_1 r + R_1 p) + I_{xz}/I_{yy}(2P_1 p - 2R_1 r) = M_u u + M_w w + M_{\dot{w}}\dot{w} + M_q q + M_{\delta_E}\delta_E$$

$$\dot{p} - I_{xz}/I_{xx}\,\dot{r} - I_{xz}/I_{xx}(P_1 q + Q_1 p) + \frac{1}{I_{xx}}(I_{zz} - I_{yy})(R_1 q + Q_1 r) = L_\beta\beta + L_p p + L_r r + L_{\delta_A}\delta_A + L_{\delta_R}\delta_R$$

$$\dot{r} - I_{xz}/I_{zz}\,\dot{p} + \frac{I_{xz}}{I_{zz}}(Q_1 r + R_1 q) + \frac{1}{I_{zz}}(I_{yy} - I_{xx})(P_1 q + Q_1 p) = N_\beta\beta + N_p p + N_R r + N_{\delta_A}\delta_A + N_{\delta_R}\delta_R$$

where in these relations the $(\cdot)_1$ quantities (e.g., U_1, V_1, W_1) are constant, steady-state values, and X_w, Z_w, etc. are the dimensional stability deriva-

*Roskam, J., Flight Dynamics of Rigid and Elastic Airplanes, Lawrence, Kansas, 1979.

tives (see the above reference).

The case to be evaluated consists of a level, 4-g ($n = 4$) turning condition at 10,000 ft. altitude, Mach = 0.72. Therefore, for this case, the steady-state parameters are given as follows (equations developed in the aircraft stability axis)

$$\Theta_1 = 0.$$

$$U_1 = V = 775 \text{ ft/sec} \qquad \cos \Phi_1 = \frac{1}{n} = \frac{1}{4}$$

$$V_1 = W_1 = 0. \qquad \Phi_1 = 75.52 \text{ deg.}$$

Turn rate, $\dot{\Psi} = g(\tan \Phi_1)/U_1 = .161$ rad/sec.

Roll rate, $P_1 = 0$

Pitch rate, $Q_1 = \dot{\Psi} \sin \Phi_1 = .156$ rad/sec

Yaw rate, $R_1 = \dot{\Psi} \cos \Phi_1 = .040$ rad/sec.

The angle of attack required for trim (Ref.) is 14.5° and the elevator deflection for trim is -20 deg at this altitude and velocity. The inertias (in the body axis) are

$$I_{xx} = 2.126 \times 10^4 \text{ slug-ft}^2$$

$$I_{yy} = 2.035 \times 10^5 \text{ slug-ft}^2$$

$$I_{zz} = 2.175 \times 10^5 \text{ slug-ft}^2$$

$$I_{xz} = 7.316 \times 10^3 \text{ slug-ft}^2$$

The reference wing area is 695 ft^2 and the weight is 33,000 pounds. In the stability axis, the inertias are

$$I_{xx_s} = 2.999 \times 10^4 \text{ slug-ft}^2$$

$$I_{zz_s} = 2.088 \times 10^5 \text{ slug-ft}^2$$

$$I_{xz_s} = -4.111 \times 10^4 \text{ slug-ft}^2$$

Finally, the dimensional derivatives are estimated to be (for c=m.a.c. = 23.8 ft)

$X_u = -.0924\ (sec^{-1})$ $\quad Y_\beta = -177.\ (ft/sec^2)$

$X_\alpha = -176.0\ (ft/sec^2)$ $\quad Y_p = 1.76\ (ft/sec)$

$X_{\delta_E} = -24.4\ (ft/sec^2)$ $\quad Y_r = 8.13\ (ft/sec)$

$Z_u = -.437\ (sec^{-1})$ $\quad Y_{\delta_A} = 84.9\ (ft/sec^2)$

$Z_\alpha = -987.\ (ft/sec^2)$ $\quad Y_{\delta_r} = 36.5\ (ft/sec^2)$

$Z_{\delta_E} = -288.\ (ft/sec^2)$ $\quad L_\beta = -47.6\ (sec^{-2})$

$M_u = -.00223\ (ft^{-1}sec^{-1})$ $\quad L_p = -.0613\ (sec^{-1})$

$M_\alpha = -11.5\ (sec^{-2})$ $\quad L_r = 2.77\ (sec^{-1})$

$M_{\dot{\alpha}} = -.785(.3485)(sec^{-1})$ $\quad L_{\delta_A} = -57.4\ (sec^{-2})$

$M_q = -.785(.3485)(sec^{-1})$ $\quad L_{\delta_R} = .567\ (sec^{-2})$

$M_{\delta_E} = -17.36\ (sec^{-2})$ $\quad N_r = -.842\ (sec^{-1})$

$N_\beta = 6.77\ (sec^{-2})$ $\quad N_{\delta_A} = -5.93\ (sec^{-2})$

$N_p = -.176\ (sec^{-1})$ $\quad N_{\delta_R} = -3.98\ (sec^{-2})$

Finally, in the steady-state condition being considered, the aileron/rudder interconnect results in the following relation

$$\delta_R = \delta_{R\ commanded} - 1.1\delta_A$$

In addition, the feel system for this vehicle is estimated to provide the following stick gains

$$\delta_E = .0467\ \delta_{E_{stick}}\ (in.) \qquad \delta_A = .0273\ \delta_{A_{stick}}\ (in.)$$

$$\delta_R = .0738\ \delta_{R_{ped}}\ (in.)$$

Combining all above parameters, the resulting vehicle dynamics in this turning condition are expressed as

$$\dot{u} = .0924\,u - 297.\alpha - 32.2\theta + 31.2\beta - 1.14\delta_{E_{st}}$$

$$\dot{\alpha} = -.00036\,u - 1.272\alpha + q - .040\phi - .0173\delta_{E_{st}}$$

$$\dot{q} = -.00013\,u - 11.21\alpha - .547q + .0109\phi + .0353\,p - .0162r - .806\delta_{E_{stick}}$$

$$\dot{\beta} = -.228\beta + .0104\phi + .00227p - .99r - .00005u + .00156\delta_{A_{st}} + .00347\delta_{R_{ped}}$$

$$\dot{p} = -.0245q - 77.9\beta + .198p + 5.27r - 2.091\delta_{A_{st}} + .608\delta_{R_{ped}}$$

$$\dot{r} = .0127q + 22.1\beta - .344p - 1.852r + .370\delta_{A_{st}} - .413\delta_{R_{ped}}$$

In addition to the vehicle dynamic model, the vehicle kinematics are described by the perturbation relations

$$p = \dot{\phi} - \dot{\Psi}_1\,\theta$$

$$q = \dot{\theta}\cos\Phi_1 + \dot{\Psi}_1\,\phi\cos\Phi_1 + \dot{\psi}\sin\Phi_1$$

$$r = -\dot{\Psi}_1\,\phi\sin\Phi_1 + \dot{\psi}\cos\Phi_1 - \dot{\theta}\sin\Phi_1$$

In our case, solving for $\dot{\theta}$, $\dot{\phi}$, and $\dot{\psi}$ yields

$$\dot{\phi} = p + .161\theta$$

$$\dot{\theta} = -.161\phi + .25q - .968r$$

$$\dot{\psi} = .968q + .25r$$

APPENDIX E

SYSTEM STATE VARIABLE MODEL

SYSTEM DYNAMICS ARE: XDOT=AX+BU+EW, Y=CX+DU

A MATRIX:

0	0	0	0	-.9680	0	0
0	-.2500	0	0	0	0	0
-48.02	-110.6	0	0	0	0	0
-302.0	-710.0					
0	0	0	0	0	0	0
-12.59	29.25	0	0	710.0	0	0
-78.00						
0-40.0000E-03	-.1290	0	0	-309.0	78.00	
0	0	0	100.0	0	0	31.00
0	0	50.0000E-05	77.0000E-06	-63.0000E-04	10.0000E-03	
		0	-.3875	1.000	0	
38.7000E-03	-10.0000E-03					
0	0	0	0	0	0	0
-50.0000E-05	-50.0000E-07	-19.0000E-06	10.0000E-03	-63.0000E-04		
		0	38.7500E-04	0	-.3875	
-.1290	-1.000					
0	0	0	0	0	0	0
-10.0000E-04	-.1610	0	0	.2500	0	0
0	-.9680					
0	0	0	0	0	0	0
.1610	0	0	0	0	0	0
-1.000						
0	0	0	0	0	0	0
	0-40.2500E-03	-1.272		1.000		
0	0	0	0	0	0	0
	0 10.9000E-03	-11.21		-.5470		
35.0000E-03	-16.0000E-03					
0	0	0	0	0	0	0
	0 10.4000E-03		0	0	-.2280	
22.7000E-04	-.9890					
0	0	0	0	0	0	0
-.1980	5.270	0	0	0-24.5000E-03	-77.94	
0	0	0	0	0	0	0
-.3440	-1.650	0	0	12.7000E-03	22.13	

OPEN-LOOP EIGENVALUES:

-5.4971E-03	-.1588	0
-5.4971E-03	.1588	
5.1838E-03		
-1.0058E-03		
-7.7934E-17		
-.4318	4.776	
-.4318	-4.776	
-6.6892E-03	-.1592	
-6.6892E-03	.1592	
-.4094	3.329	
-.4094	-3.329	
-1.004		0

B MATRIX:

-17.3000E-03								
-.8560								
0	29.6000E-04	34.7000E-04						
0	-1.643	.6886						
0	.2010	-.4130						

C MATRIX:

57.1000E-04	0	39.3000E-05	0	1.000	0	0	0	0
	-12.8000E-04	0	-.2480	0	0	0	0	0
0	0	50.0000E-05	77.0000E-06	-63.0000E-04	10.0000E-03	0	0	0
	-49.3000E-04	-20.0000E-04	-77.5000E-03	1.506		0	0	0
	87.0000E-04	-10.0000E-03						
-76.8000E-05	39.3000E-05	-39.3000E-07	0	0	1.000	0	0	0
	-75.0000E-04	-18.3000E-03	30.5000E-04	0	-.2490	0	0	0
0	50.0000E-05	-50.0000E-07	-19.0000E-06	10.0000E-03	-63.0000E-04	0	0	0
	-19.0000E-03	-46.0000E-03	87.5000E-05	23.0000E-05	-.4450	0	0	0
	-.2480	-1.037						
-57.1000E-04	0	-39.3000E-05	0	17.7000E-04	0	0	0	0
	12.8000E-04	0	.2480	0	0	0	0	0
0	0	0	0	0	0	0	0	0
	49.4000E-04	20.0000E-04	-.3100	-.5960		0	0	0
	30.0000E-03							
76.8000E-05	-39.3000E-05	39.3000E-07	0	0	17.7000E-04	0	0	0
	75.0000E-04	18.3000E-03	-30.5000E-04	0	.2490	0	0	0
0	0	0	0	0	0	0	0	0
	19.0000E-03	46.0000E-03	30.0000E-04	-23.0000E-05	-58.0000E-03	0	0	0
	.1190	37.0000E-03						
0	0	0	0	0	0	0	0	0
	-3.550	59.830		0	94.3000E-03	-225.0	0	0
0	0	0	0	0	0	0	0	0
		1.000						

D MATRIX:

0	0	0	
43.0000E-04	0	0	
-52.8000E-06	-73.8000E-05	-16.4000E-04	
-43.0000E-04	0	0	
52.8000E-06	73.8000E-05	16.4000E-04	

APPENDIX F

MANAGEMENT SUMMARY

Summarized in this appendix is the list of written publications, including those planned; data on the advanced degree student supported by this research; and the summary of conference papers presented and interactions with the Air Force Wright Aeronautical Laboratories (formerly the Flight Dynamics Lab).

Publications include the following:

1) D.K. Schmidt, "Pilot-Optimal Augmentation for the Air-to-Air Tracking Task," to appear in the AIAA Journal of Guidance and Control, 1980.

2) S.N. Prasad and D.K. Schmidt, "Closed-Loop Pilot/Vehicle Analysis for Multi-Axis Air-to-Air Tracking," in preparation for submission to the AIAA Journal of Guidance and Control.

One graduate student was supported for one semester and one summer session on this program and much of the technical results herein are included in his thesis. This student, Mr. S.N. Prasad, will receive the Master's Degree in Aeronautical and Astronautical Engineering from Purdue University in August, 1980, and his M.S. thesis will be published at that time.

Other dissemination of this studies results has been accomplished via papers presented at technical conferences. These include presentation of the first paper cited above at the 1979 AIAA Guidance and Control Conference held at Boulder, Colorado, August 6-8, 1979. In addition, a presentation entitled "Multi-Axis Tracking Via an Optimal Control Pilot Model," was made at the 16th Annual Conference on Manual Control at Cambridge, Mass. in May, 1980.

Finally, throughout the course of this program, frequent contacts have been made with the members of the technical staff of the Flight Control Division, Air Force Wright Aeronautical Laboratories (formerly the Flight Dynamics Laboratory). These contacts have included participation in workshops (1979 Flying Qualities Symposium, October, 1979, and the 1980 Stability and Control Workshop, April, 1980) held at Wright-Patterson AFB, Ohio. Also, informal telephone contacts with Mr. Ronald O. Anderson and Mr. Frank George of the Wright Aeronautical Laboratories have been made a number of times throughout this study.